Exploring Copper as a Catalyst for Supercritical Fluid-Based Silicon Nanowire Growth

Saibihai Rousidan

A thesis

submitted in partial fulfillment of the

requirements for the degree of

Master of Science in Chemical Engineering

University of Washington

2018

Committee:

Vincent C. Holmberg

Qiuming Yu

Program Authorized to Offer Degree:

Chemical Engineering

University of Washington

Abstract

Exploring Copper as a Catalyst for Silicon Nanowire Growth

Saibihai Rousidan

Chair of the Supervisory Committee:
Assistant Professor Vincent C. Holmberg
Department of Chemical Engineering

Silicon Nanowires (SiNWs) have numerous potential applications in many different fields. Herein, we report the semi-continuous supercritical fluid-solid-solid (SFSS) growth of Cu-seeded SiNWs. Homogeneous nucleation of silicon precursor is strongly influenced by the reaction temperature and has a huge impact on achieving continuous steady-state growth of SiNWs. We also demonstrate that by tuning the overall precursor concentration and precursor-to-metal seed ratio, one can suppress the homogeneous nucleation and reduce defects. In addition, we present an approach that can be adapted to integrate different materials into backbone/branch heterostructures. This strategy provides additional control over nanostructure morphology, offering a handle to explore and design nanowire-based structures for various applications.

TABLE OF CONTENTS

List of Figures iii

Chapter 1. Introduction & Background 1

Chapter 2. Copper Seeded Silicon Nanowire Growth 5

2.1 Introduction 5

2.2 Experimental Methods 8

2.2.1 Copper Nanocrystal Synthesis (DDA-Capped) 8

2.2.2 Copper Nanocrystal Synthesis (TDPA-Capped) 9

2.2.3 Silicon Nanowire Synthesis 10

2.2.4 Characterization Methods 12

2.3 Results and Discussion 13

2.4 Conclusions 19

Chapter 3. Single-Crystalline Branched Silicon Nanowires 20

3.1 Introduction 20

3.2 Experimental Methods 22

3.2.1 Materials and Reagents 22

3.2.2 Two-Step Synthesis of Branched Silicon Nanowires 22

3.2.3 Characterization Methods 23

3.3 Results and Discussion 24

3.4 Conclusions 30

References 31

Appendix A 38

Appendix B.. 40

LIST OF FIGURES

Figure 1.1 Schematic of VLS growth 2
Figure 2.1 Measured ionization energies for various impurities in silicon 6
Figure 2.2 Logarithm of D versus 1/T(K) curves for the diffusion of Cu, Au, Ag and Al in Si 7
Figure 2.3 The SFLS/SFSS nanowire growth reactor system[98] 12
Figure 2.4 TEM and HRTEM images of CuNCs 14
Figure 2.5 Cu/Si binary phase diagram 15
Figure 2.6 SEM images of Cu-seeded SiNWs 16
Figure 2.7 EDS mapping of Cu-seeded SiNWs 17
Figure 2.8 TEM images of Cu-seeded SiNWs 18
Figure 3.1 Schematic illustration of Au/Cu-seeded branch SiNW growth 24
Figure 3.2 SEM images of Au-seeded SiNWs 25
Figure 3.3 TEM images of Cu_3Si forming on Au-seeded SiNW backbone 26
Figure 3.4 SEM images of single branched SiNW 27
Figure 3.5 TEM images of branched SiNWs 27
Figure 3.6 TEM and HRTEM of Cu-seeded SiNW branches ..... **Error! Bookmark not defined.**

ACKNOWLEDGEMENTS

Dedicated to my life-coach, my mother Sabira Sidik: because I owe it all to you. Many Thanks!

A very special gratitude goes to my forever interested, encouraging, and always enthusiastic advisor Vincent Holmberg. Without you, I might not have reached the level I am today. Thanks for being not only my advisor in research, but also a very strong supporter to help me through my struggles.

I am grateful to our graduate student coordinator, Allison Sherrill, who has provided me with moral and emotional support in the toughest moment of my life. Your kindness is the greatest thing that eases the pressure and struggle of graduate school.

With a special mention to Grant Williamson, Elena Pandres, Nicole Thompson, Soohyung Lee, Brittany Bishop, the support team, and friends in general. It was fantastic to have the opportunity to work with all of you. What a talented group of people to work with!

And finally, last but by no means least, also to everyone in the Benson basement… it was great sharing laughter and joy with all of you during rainy Seattle winters.

Thanks for all your encouragement!

Chapter 1. INTRODUCTION & BACKGROUND

Since the late 1990s, the study of semiconductor nanowires (NWs) has become one of the most active research areas within the nanoscience community. To date, numerous studies have been carried out to explore nanowires as new building blocks in transistors[1]–[8], chemical/biological sensors[9]–[12], photovoltaic devices[13]–[17], and batteries[18]–[24] to name a few examples.

To improve the physical characteristics of NWs in each of these specific applications, understanding the fundamental principles associated with NW synthesis becomes critical. Through an improved understanding of the structure-property-application relationship, one can obtain knowledge in synthesis which advances one's capability to uniformly manipulate NW-based structures. A better understanding of synthesis can also increase product yield, and thus improve cost control in manufacturing. In addition, robust structural modification techniques can allow one to create structures with novel properties, leading toward more innovative NW applications. In seeded nanowire growth, the choice of metal catalyst can have great impact on the characteristics of the resulting nanowires.

There are many different methods of making semiconductor nanowires, but all production strategies can be broadly grouped into two categories: either bottom-up or top-down approaches. Top-down approaches, which are widely used in the semiconductor chip manufacturing industry, rely on dimensional reduction through selective etching and nanoimprinting techniques. Bottom-up growth methods, although not yet widely used in commercial settings, offer the promise of improved control and reduced waste relative to top-down methods. Starting with individual atoms and molecules, bottom-up approaches enable the ability to obtain high quality nanowire

heterostructures, including core-shell radial heterostructures[20],[24]–[31], axial heterostructures[32]–[40], and branched 3D structures[8], [18], [19], [30], [41]–[57], thus opening up the possibility of a whole new set of nanowire applications.

The vapor-liquid-solid (VLS) bottom-up growth process, due to its simple realization and flexible and excellent control over many aspects of the synthesis process, became the most widely adopted approach to grow semiconductor nanowires. Typical VLS growth involves alloying, nucleation, and growth stages. As shown in Figure 1.1, the process starts with a pure metal catalyst. A gaseous precursor reacts at the heated catalyst surface, and a component of the precursor alloys with the catalyst. As the alloy particle becomes supersaturated, the precursor component then precipitates from the solid-liquid interface to form a nanowire. Depending on the choice of catalyst, the material may undergo vapor-solid-solid (VSS) growth instead of VLS-based growth. The basis of the VSS growth mechanism is the solid state of the metal alloy tip during growth, as opposed to the liquid alloy droplet employed in the case of VLS growth.

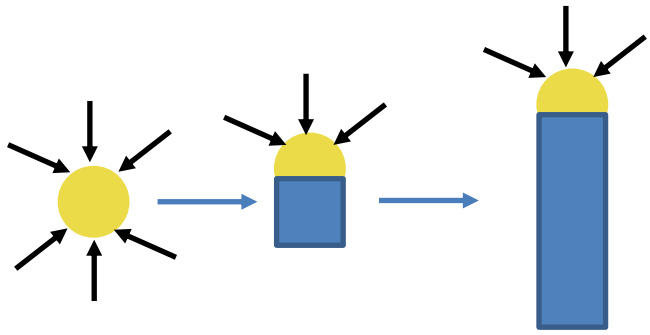

Figure 1.1 Schematic of VLS growth

There are also many methods to synthesize nanowires in the solution phase rather than the gas phase. These include solution-liquid-solid (SLS), supercritical fluid-liquid-solid (SFLS), and supercritical fluid-solid-solid (SFSS), for example. Growing with a solution-based method offers the potential for increased throughput and eliminates the need for expensive vacuum-based

techniques, thus reduces overall cost. The nanowires investigated herein were grown using a 10 mL flow-through supercritical fluid reactor. Supercritical toluene was used as the solvent, because it is a volatile, low-cost organic solvent, which facilitates easier and cheaper processing relative to the oily, expensive high boiling point solvents used in most high-temperature, solution-based, air-free syntheses. The ability to continuously introduce precursor solution into the reactor, due to its flow-through design, helps to increase nanowire production throughput relative to batch syntheses. In addition, the design is readily scalable and has been shown to reach production rates on the order of grams per hour with a larger 200 mL reactors.

Silicon is one of the most abundant elements on earth. As a semiconductor, silicon is used to make transistors, which amplify or switch electrical currents and are the backbone of electronic devices ranging from radios to computers. With its enormous storage capacity, silicon would also potentially have decisive advantages over the electrode materials traditionally used in commercially available lithium-ion batteries[20], [21], [58]–[63]. In fact, silicon is one of the highest-capacity negative electrode materials, and can store up to 10 times more energy than the graphite anodes employed in conventional lithium-ion batteries. However, silicon goes through over 300% volume expansion during lithiation, and then contracts again during de-lithiation. This expansion produces stress and strain on the silicon material, causing cracks and breakage that leads to electrical disconnection[58]–[62]. Reducing the dimensions of the active material to the nanoscale regime is an effective approach. Facile strain relaxation in nanowires allows for expansion along the nanowire diameter without cracks or breaks forming, thus effectively accommodate volume expansion during cycling while withstanding the strain that would typically cause electrode pulverization[58].

Increasing the dimensionality of nanowire-based structures provides potential for a higher degree of complexity. Increasing the number of connection points, and providing a means for parallel connectivity and interconnection of functional elements, increases the potential for nanowire applications. In recent years, several advanced branched nanowire morphologies have been achieved, with helical nanotree growth[42], [64], hyper-branch growth[18], [19], [41], [65], [66], oscillation of the branch diameter[67], [68], and designed branch placement[55]–[57] being reported.

This thesis is divided into two main parts. In the first half, we focus on using copper as a seed to grow silicon nanowires in order to resolve several critical problems associated with using expensive gold catalysts for silicon nanowire growth. In second half of this thesis, we report the growth of branched silicon nanowires with crystallographic registry by applying a stepwise seeding strategy in the supercritical fluid reactor. In addition, we show a simple one-step synthesis procedure for the growth of single-crystalline SiNWs. Further background discussion is also included in each chapter.

Chapter 2. COPPER SEEDED SILICON NANOWIRE GROWTH

2.1 INTRODUCTION

One-dimensional (1D) nanomaterials have high surface area, which makes them appealing candidates for certain applications, as mention above. This characteristic, combined with considerably different electronic[69]–[71], mechanical[70], [72], [73] and optical[14]–[16] properties, as compared to bulk materials, makes nanomaterials particularly interesting. Thanks to researchers all around the world, different methods and techniques have been developed to enable control over the physical, chemical, and electronic properties of nanowires. These techniques are not simply limited to controlling the diameter and length of the wires, but also include adding additional functionality by creating core-shell nanowire heterostructures[46]–[50], axial nanowire heterostructures[36], [37], [77]–[80], branched nanowire heterostructures[18], [19], [41], [65]–[68], nanoparticle-decorated nanowire heterostructures[81]–[84] and functionalized nanowire heterostructures[85]–[88]. All of these strategies provide additional handles to explore the wide field of applications for these materials. However, their practical implementation may potentially be limited due to manufacturing cost, among other concerns. Hence, the study of cost-effective semiconductor materials that are comprised of earth abundant elements and environmentally sustainable materials has great importance.

Gold is the most frequently used catalyst for nanowire synthesis in general, especially for silicon nanowire synthesis. Due to certain advantages, gold can be considered as a well-suited catalyst. The gold and silicon binary phase diagram has a eutectic point at a relatively low temperature. This low-temperature eutectic point allows for growth and processing temperatures as low as 360 °C. Also due to the relatively high solubility of silicon at the eutectic point, the

growth process is robust with respect to fluctuations of the silicon precursor concentration [89]. There are additional concerns that make gold a non-ideal catalyst for silicon nanowire growth; however, even if those concerns were addressed, gold is still an extraordinarily expensive catalyst material choice. Using expensive catalysts necessarily increases the production price of the nanowires, reducing the range of applications that are potentially commercially viable. Also, gold is prohibited in clean rooms, which makes the nanowire production process not easily translatable to the current semiconductor production industries. This will once again become a barrier to the real-world application of semiconductor nanowires.

The most severe drawback of using gold as a catalyst is that Au can be incorporated into the nanowires as a result of contact between the liquid AuSi alloy and the crystalline semiconductor at high temperature during growth. As shown in Figure 2.1, gold impurities in in silicon introduce electronic levels that sit deep within the band gap of silicon, acting as device-killing electron traps.

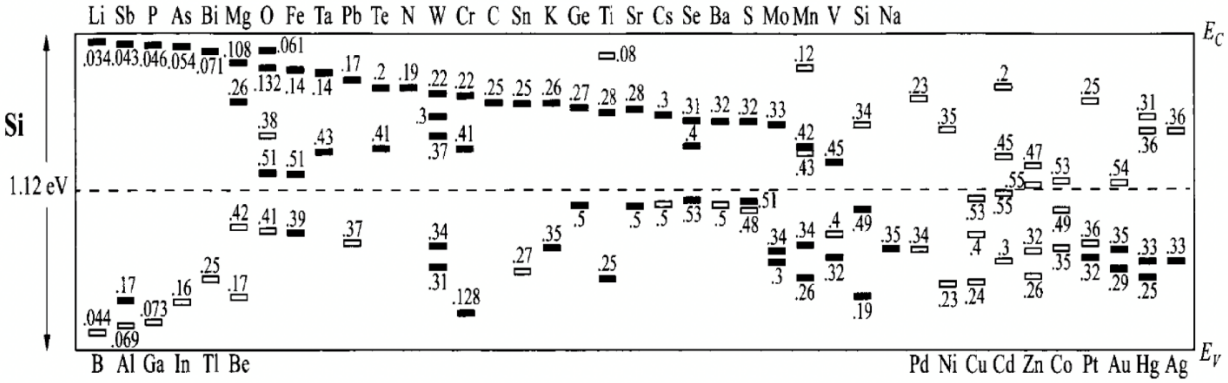

As an alternate strategy, Kayes*, et al*. has reported growth of vertically aligned Si wire arrays over large areas using Cu as catalyst during vapor-based wire growth.[90] Unlike gold, copper is

relatively cheap and much more abundant, which makes it more appealing for study in terms of potential cost effectiveness.

Surprisingly, despite the high diffusivity of copper in silicon (Figure 2.2), and the fact that both gold and copper impurities have deep trap states, literature suggests that Si solar cells are much more tolerant to Cu contamination than to Au[91]–[93]. Moreover, Cu incorporation in SiNWs is of potential interest for improving performance in lithium-ion batteries[94].

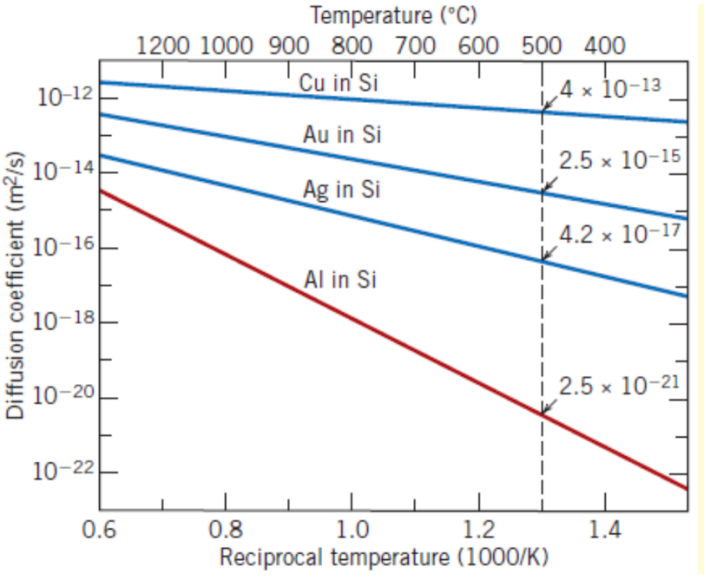

Figure 2.2 logarithm of D versus 1/T(K) curves for the diffusion of Cu, Au, Ag and Al in Si

Chemical vapor deposition (CVD)-based NW growth typically requires vacuum-based batch processes and often results in only a few micrograms of product, making it difficult to scale in a cost-effective manner. Without the ability to scale new technologies, a gap persists between lab-scale syntheses and commercial viability. As discussed above, using supercritical fluid-based synthesis leads to much greater yield per time of semiconductor nanowires relative to vapor-based syntheses, and thus has the potential to make the process more scalable. Moreover, Constantinou

et al. [95] have demonstrated that the combination of dielectrophoresis (DEP) and impedance spectroscopy can be used to isolate, select, and separate the population of NWs with the highest conductivity and lowest defect density from a batch of nanowires that may contain a wide spectrum of conductivities and defects (as is typically the case with Au-seeded silicon nanowires), thus enabling researchers to achieve the tunable selection of wires with a desired set of properties. All of this has made the idea of using colloidal copper nanocrystals as seeds, using the scalable supercritical fluid-based growth method, and potentially increasing the population of high quality, defect-free silicon nanowires a promising research topic for study. Developing a SFSS-based growth of Cu-seeded SiNWs will require finding optimal growth parameters, including overall precursor concentration, precursor-to-nanocrystal seed ratio, and precursor decomposition kinetics.

2.2 Experimental Methods

An inert-atmosphere, nitrogen-filled glove box (H_2O < 0.5 ppm, O_2 < 0.5 ppm) was used to store and handle all air- and moisture-sensitive chemicals. All copper nanocrystal syntheses were carried out under nitrogen atmosphere using standard Schlenk line techniques.

2.2.1 *Copper Nanocrystal Synthesis (DDA-Capped)*

Materials

1-Dodecylamine (≥ 99%), copper (II) chloride (97%), triphenylphosphine (97%), borane tert-butylamine complex (97%), toluene (anhydrous, 99.8%), ethanol (anhydrous, ≤0.005% water), and oleic acid (degassed, 90%) were purchased from Sigma-Aldrich. Ethanol (200 proof) was purchased from Decon Laboratories. All chemicals were used as received, without further purification.

Methods

1-Dodecylamine (DDA)-capped copper nanocrystals were prepared by the method of Ben Aissa *et al*.[96] In a typical synthesis, 0.25 mmol of $CuCl(PPh_3)_3$ complex is dissolved in 25 mL of anhydrous toluene in a glovebox under a nitrogen atmosphere. The solution is then injected to a three-neck round-bottom flask connected to a Schlenk line and heated to 100°C. 520 μL of 1-dodecylamine (DDA) is quickly injected into the solution under vigorous stirring. In parallel, a second solution is prepared by dissolving 2.5 mmol of the tert-butylamine borane (TBAB) complex in 15 mL of anhydrous toluene and is heated to the same temperature. The injection of TBAB takes place 10 minutes after the injection of DDA in order to allow the first solution to stabilize at the desired temperature. The reaction proceeded at this temperature for 60 minutes. Afterward, the reaction is stopped by cooling the solution to room temperature and injecting 400 μL of oleic acid (OA), followed by another 5 minutes of stirring. Nanocrystals are then transferred to 4 vials in the glovebox and washed by the addition of 10 mL of ethanol, followed by centrifugation at 4500 rpm for 10 min. The supernatant is discarded, and the precipitate was dispersed in 10 mL of anhydrous toluene.

To synthesize the copper precursor complex used in this synthesis, 22.28 g of triphenylphosphine (PPh3) is dissolved in 380 mL of ethanol and slowly heated under stirring until the triphenylphosphine is dissolved. Then, 2.68 g of copper (II) chloride is progressively added. The heterogeneous mixture is stirred for ten minutes and cooled to room temperature. The solution is filtered, and the resulting $CuCl(PPh_3)_3$ powder is washed several times with ethanol. Then it is dried under vacuum and kept in the glovebox.

2.2.2 *Copper Nanocrystal Synthesis (TDPA-Capped)*

Materials

1-Tetradecylphosphonic acid (97%) was purchased from Epsilon Chimie. Trioctylamine (98%), copper (I) acetate (97%), ethanol (anhydrous, ≤0.005% water), and hexane (anhydrous, 99.8%) were purchased from Sigma-Aldrich. All chemicals were used as received, without further purification.

Methods

12-nm diameter copper nanocrystals capped with 1-tetradecylphosphonic acid (TDPA) were prepared by the method of Hung *et al*.[97] First, Trioctylamine (TOA) was heated to 130°C inside a three-neck flask for 30 minutes under a flow of nitrogen in order to remove water and any dissolved oxygen, and then transferred into the glovebox for further use. In the glovebox, 1 mmol copper (I) acetate (0.12259 g) and 1 mmol 1-tetradecylphosphonic acid (TDPA) (0.27838 g) were added to 10 mL of TOA in a three-neck round-bottom flask, transferred to the Schlenk line, purged with nitrogen, and stirred at 1200 rpm to fully dissolve the components. The solution was rapidly heated to 180°C and maintained at that temperature for 30 minutes in order to form the necessary organometallic precursor complex. The temperature was then increased to 270°C and held at this temperature for another 30 minutes. After the reaction is completed, the solution is cooled to room temperature and transferred to the glove box. Copper nanocrystals were washed by the addition of 8 mL of ethanol, followed by centrifugation in the glove box at 4500 rpm for 15 min. The supernatant was discarded, and the precipitate was dispersed in 20 mL of anhydrous hexane.

2.2.3 *Silicon Nanowire Synthesis*

Materials

Monophenylsilane (>95%) was purchased from Gelest. Toluene (anhydrous, 99.8%) was purchased from Sigma-Aldrich. Chloroform (HPLC grade, 99.9%), and anhydrous toluene

(Certified ACS, 99.8%) were purchased from Fisher Chemistry. Ethanol (200 proof) was purchased from Decon Laboratories.

Methods

Silicon nanowires were synthesized via SFSS growth. A typical SFSS nanowire growth system and reactor are shown in Figure 2.3[74] In a typical growth reaction, the reaction vessel was transferred into the nitrogen filled glovebox (H_2O < 0.5 ppm, O_2 < 0.5 ppm), sealed, and then transferred out and placed into the heating block at 550 °C. The reactor was then pressurized to 1500 psig with anhydrous toluene. In order to pressurize the system, the exit valve of the reactor was closed, and a high-performance liquid chromatography (HPLC) pump was used to push anhydrous toluene into the reactor. A 12 mL mixture containing a prescribed amount of copper nanocrystals and 150 mM monophenylsilane with the remaining volume consisting of anhydrous toluene was prepared inside the glovebox and loaded into a syringe. The mixture was then loaded into a 10 mL stainless-steel injection loop connected to a six-way injection valve, and subsequently injected into the pre-pressurized and pre-heated reactor (1500 psig, 550 °C) at a rate of 0.5 mL/min for 20 minutes. After nanowire growth, the reactor was removed from the heating block and cooled to room temperature. Nanowires were collected with toluene, washed three times in glass vials with a 2:2:1 ratio of toluene:chloroform:ethanol, and centrifuged at 4500 RPM for ten minutes.

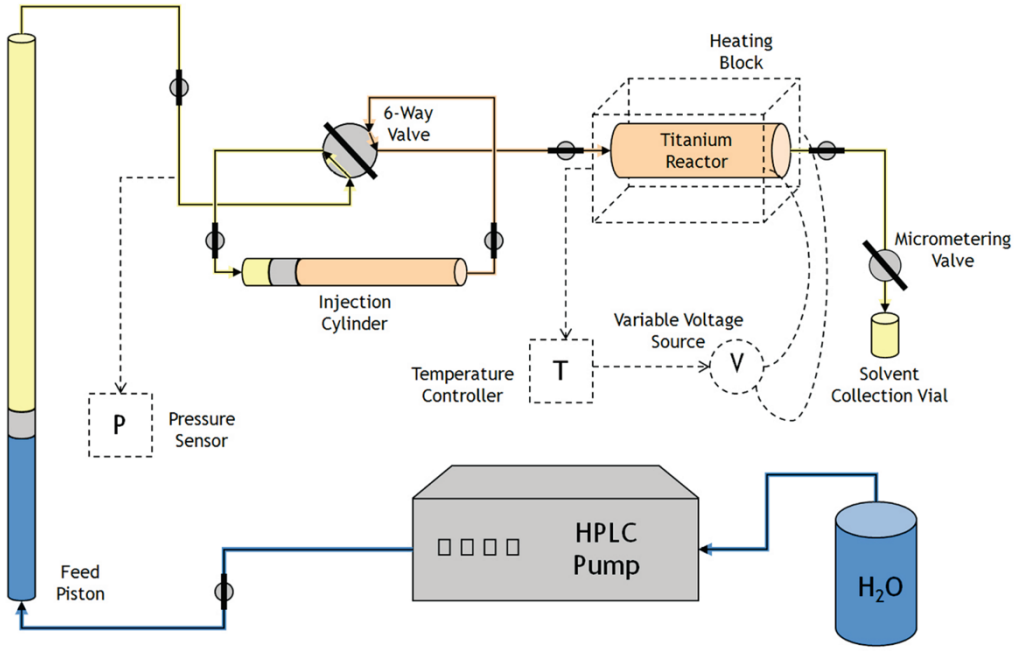

Figure 2.3 The SFLS/SFSS nanowire growth reactor system[98]

2.2.4 *Characterization Methods*

Transmission Electron Microscopy (TEM)

Transmission electron microscopy (TEM) images were acquired with a FEI Technai G2 F20 Super Twin TEM, operating at an accelerating voltage of 200 kV. Digital Micrograph software was used to analyze Fast Fourier Transforms (FFTs) of high resolution TEM images. TEM samples were prepared by dropping 8 μL of nanocrystal/nanowire dispersion on either carbon-coated copper TEM grids or carbon-coated 200 mesh nickel TEM grids (Electron Microscopy Sciences) inside of the glovebox, and allowing the organic solvent to evaporate.

Scanning Electron Microscopy (SEM)

To characterize the morphology of nanowires, scanning electron microscopy (SEM) images were acquired with a FEI XL830 Dual Beam FIB/SEM. Samples were prepared by drop casting nanowires onto pre-cleaned silicon wafer substrates and drying overnight.

Energy Dispersive X-ray Spectroscopy (EDS)

Energy-dispersive X-ray spectroscopy (EDS) was carried out using a scanning electron microscope (FEI XL830) equipped with an integrated Energy Dispersive X-ray Spectrometer (EDS) from Oxford in order to analyze the composition of the nanowires dispersed on the silicon wafer.

Inductively Coupled Plasma Atomic Emission Spectroscopy (ICP-AES)

To determine the concentration of copper nanocrystals, inductively coupled plasma atomic emission spectroscopy (ICP-AES) analysis was performed using a Perkin Elmer Optima 8300. Nanocrystals were digested in *aqua regia* prepared from ultrapure nitric acid and hydrochloric acid in a 1:3 volume ratio. Once digestion was complete, samples were diluted using deionized water. Calibrations were performed using multi-element VII ICP-AES standards obtained from EMD Millipore.

2.3 Results and Discussion

In order to study the catalytic effects of copper nanocrystals on silicon nanowire growth in the supercritical fluid-based reactor system, copper nanocrystals were synthesized using the methods of Ben Aissa *et al*.[96] Figure 2.4 shows representative TEM images of the copper nanocrystals obtained by the procedures described above. TEM analysis shows that Cu NCs are roughly spherical in shape with diameters ranging from 10 to 15 nm.

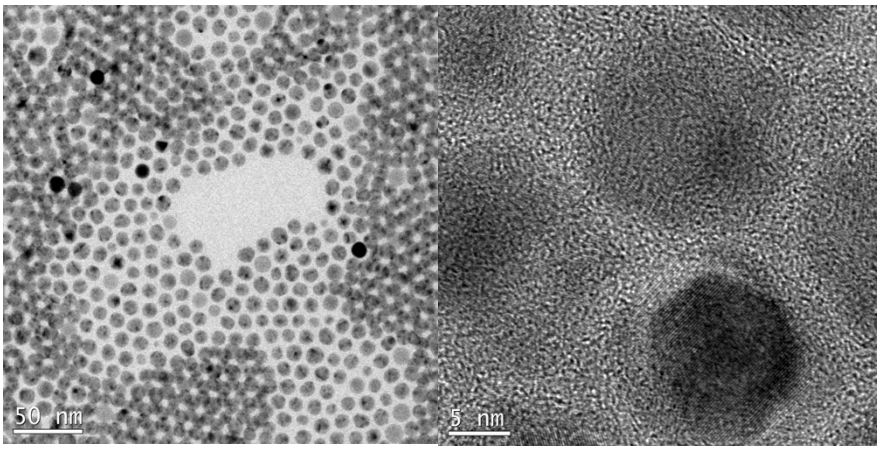

Figure 2.4 TEM and HRTEM images of CuNCs

In a screening study, Tuan *et al.*[99] reported using CuS NCs to grow SiNWs in a supercritical fluid-based growth scheme. However, they did not investigate the use of elemental copper nanocrystals in the system. Also, they only described small-scale pilot reactions with 500 μL precursor injections and did not simultaneously inject both catalyst and precursor to achieve continuous growth.

In other literature, either copper films or copper evaporated onto a silicon wafer were used as the fixed metal source. In all of the above cases, copper was present prior to the introduction of the precursors, and never co-injected. In some cases, the copper film was even preheated to form a copper silicide alloy with the silicon substrate prior to the reaction.

Preliminary experiments have demonstrated that reaction conditions do not directly translate from CVD-based growth to the supercritical fluid reactor. Results from attempts to grow SiNWs from copper foil are presented in Appendix A in Figures A.1 and Figure A.. Notably, the two faces of the copper foil appear different from one another after synthesis. The side facing upward in the reactor was coated in a thick yellow layer of polyphenylsilane that resulted from oligomerization of phenylsilane precursor, thus preventing SiNW growth. The side that faced downward toward the wall of the reactor, without a sufficient supply of silicon precursor, formed copper silicide

nanorods. Similar results also occurred when copper nanocrystal seeds were drop-cast onto the silicon wafer prior to reaction. The side facing upward was once again covered in yellow polyphenylsilane and the side facing downward received limited amounts of silicon precursor.

The decomposition of the aryl silane precursor directly affects the quality of silicon nanowires produced in the supercritical fluid reactor. If the monophenylsilane decomposes slowly, the Si concentration will not be enough to saturate the seeds and form crystalline silicon, which will result in poor-quality, highly defective nanowires. Yet, when the decomposition of the monophenylsilane increases, the homogeneous reaction of the Si precursors also increases, creating relatively high proportions of amorphous polyphenylsilane by-products[72] .

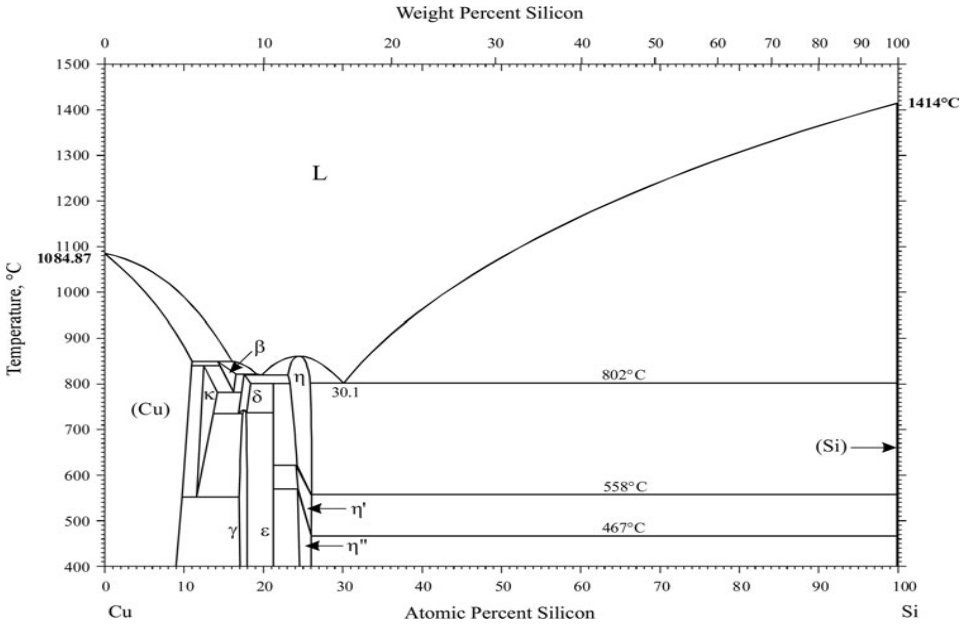

Although the decomposition temperature of monophenylsilane is relatively low,[100] the synthesis is limited by the thermally activated diffusion of Si atoms within the metal-rich solid particle.[102] Thus, growth temperatures higher than 500°C are necessary. At the chosen growth temperature of 550°C, monophenylsilane (MPS) decomposes rapidly, yet, homogeneous

nucleation can also be prevented by balancing the overall concentration and the precursor-to-metal seed ratio.

We determined the optimized growth temperature of 550°C based on a survey of the literature and our own experience experimentally. From the Cu/Si binary phase diagram (Figure 2.5), the lowest eutectic temperature is 802°C. The SiNWs therefore grow from solid-phase copper seeds. The growth pressure and MPS concentration were chosen based on Au-seeded SFLS-based growth of SiNWs. After fixing all other parameters, we gradually increased the molarity of Cu NCs in the growth solution. With the increase of seed ratio, as observed from SEM images shown in Appendix A in Figure A.3, the homogeneous nucleation was reduced, and nanowire growth increased. The existence of a large quantity of amorphous by-product made imaging difficult due to significant charging. However, further increasing the seed ratio, lead to the growth of copper-seeded silicon nanowires with minimal amorphous silicon by-products.

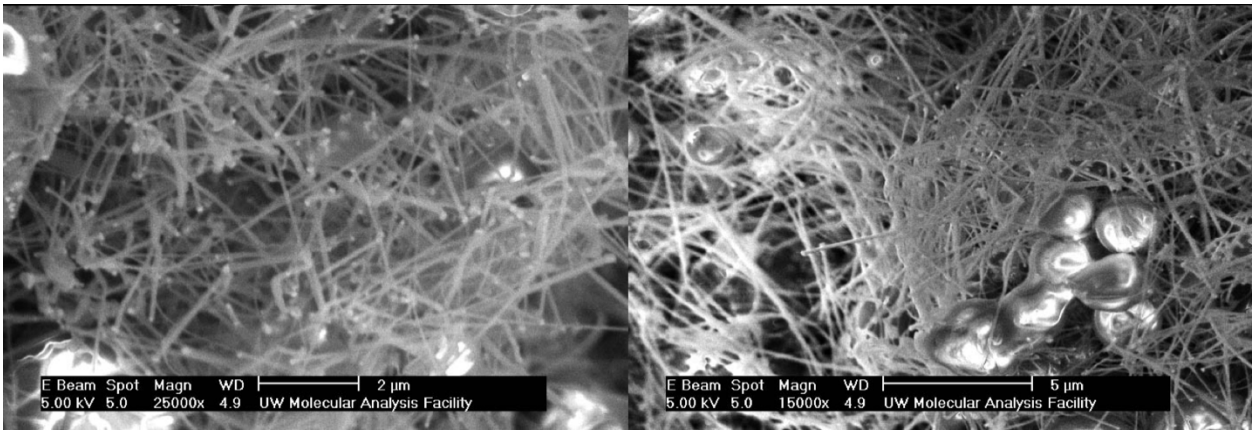

Figure 2.6 presents SEM images of the as-synthesized Cu-seeded SiNWs. Even without any post-processing, there is only a limited amount of unwanted homogeneous nucleate present, once again highlighting the advantages of using supercritical toluene as a growth media – making the resultant material much easier to clean.

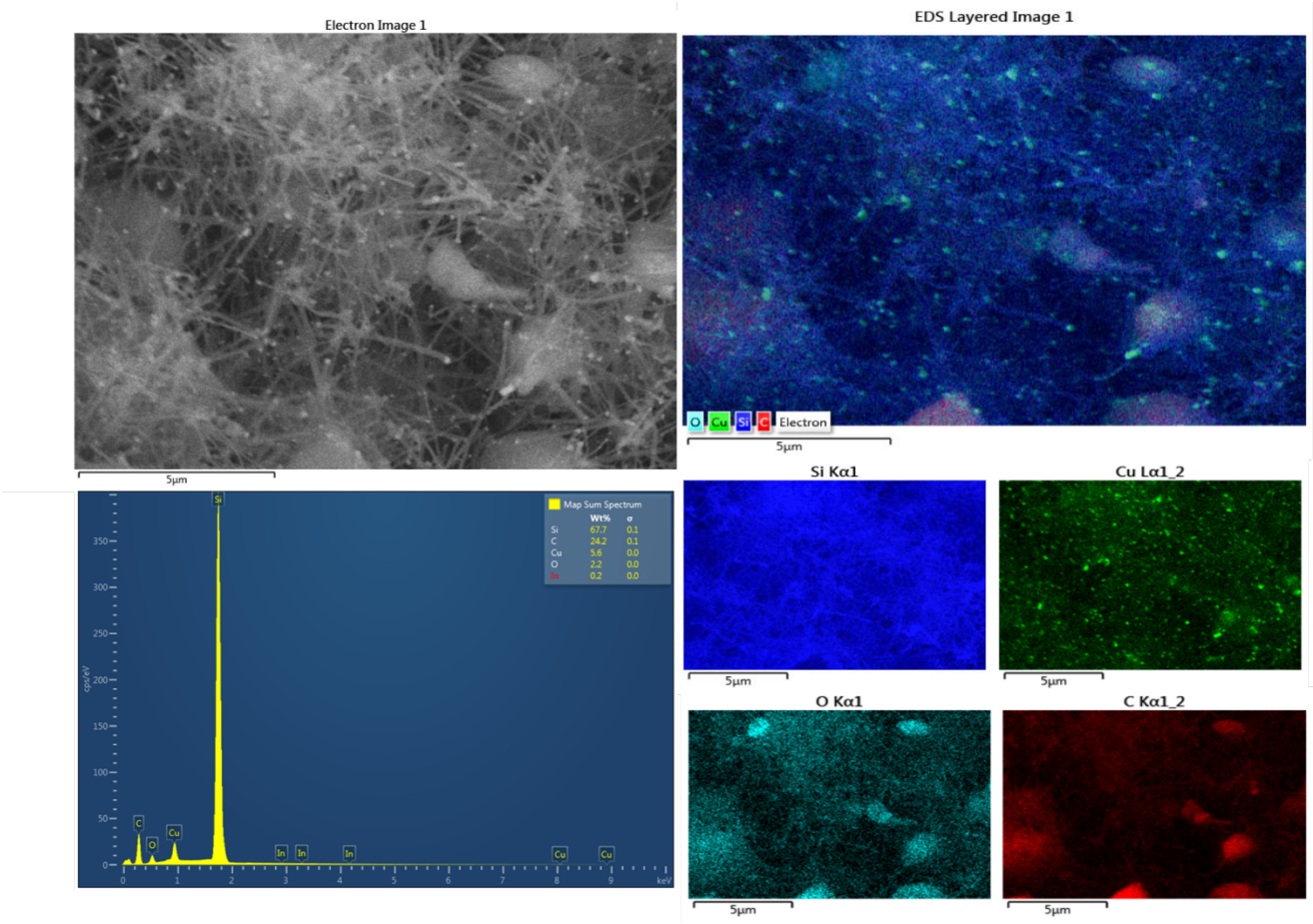

EDS measurements were also preformed to verify the chemistry of the nanowires and seeds. The results are showed in Figure 2.7. Due to the silicon substrate that was used as an imaging substrate, the weight ratio and atomic ratio in the EDS are not indicative of the actual composition. However, it is clear from the mapping results that copper is localized at the tip of the nanowires and indeed acted as a seed material for SiNW growth. Large amorphous polyphenylsilane structures consisting of strong, oxygen, carbon, and silicon signals are also present[100].

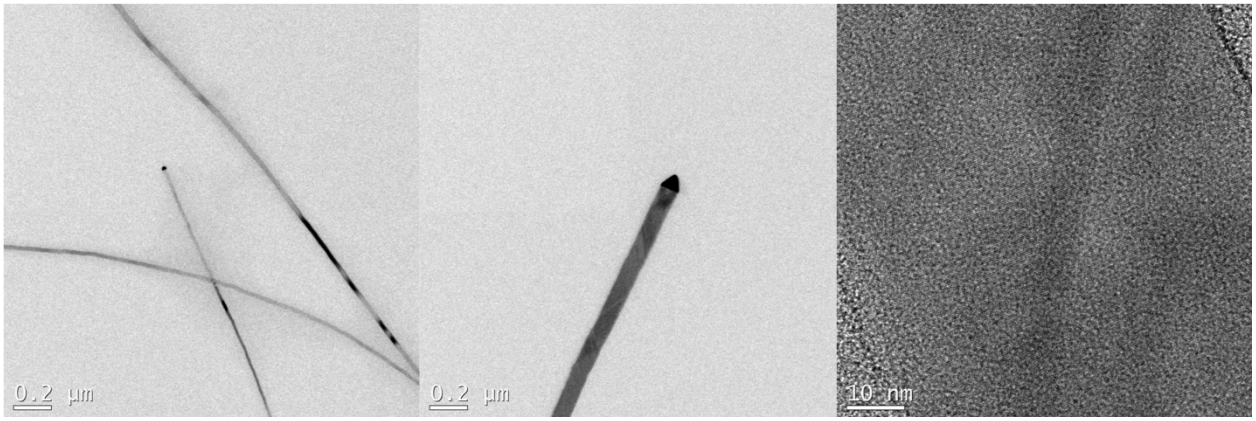

Figure 2.8 presents TEM images of the Cu-seeded Si nanowires. Both large triangular shaped tips and small round tips were observed. In solid-phase catalyst growth, normally the diameter of the nanowires is around the same size as the metal catalyst. Here the smaller round shaped tip is about the same size as the nanocrystals that were used in the reaction. However, there are also a large fraction of triangular tips in the sample that led to the wires with diameters greater than 100 nm. For catalyst particles larger than 10 nm, the melting temperature of copper is not expected to be reduced to 550°C [103]. Therefore, we ascribe the formation of triangular seeds to aggregation and subsequent alloying to form large copper silicide structures.

Electrostatic charging of dispersions of the resultant SiNWs was also observed. When a glass vial containing a dispersion of nanowires is contacted with a charged nitrile glove, the nanowires are repelled by the electrostatic charge and rapidly migrate to the walls. Without further analysis, this qualitative result suggests that the dielectrophoretic (DEP) method of Constantinou *et al*. [95] for separation and alignment of NWs from heterogeneous stock can be applied to the SFSS-grown copper-seeded SiNWs produced in this study.

2.4 CONCLUSIONS

We reported the semi-continuous SFSS-based growth of Cu-seeded SiNWs. The homogeneous nucleation of silicon precursor is strongly affected by the temperature and has huge impact on achieving continuous steady-state growth of SiNWs. We also have shown that by tuning the overall concentration and precursor-to-metal seed ratio, one can suppress the amount of homogeneous nucleation and reduce nanowire defects.

The resultant nanowires have two distinct catalytic tips. The round, small tips that are observed are around the same size as the CuNCs that were used in the growth solution. This agrees with what literature suggests about solid-state growth of nanowires. However, we also observed large, triangular shaped catalytic tips, which are hypothesized to be due the aggregation and subsequent alloying to form large, triangular copper silicide structures. Lastly, we have shown that copper-seeded SiNWs dispersed in toluene respond to electrostatic charges and thus should be amenable to the dielectrophoretic separation techniques developed by *Constantinou et al*. [95]

Chapter 3. SINGLE-CRYSTALLINE BRANCHED SILICON NANOWIRES

3.1 INTRODUCTION

In this section, we report the formation of colloidally grown branched silicon nanowires by applying a stepwise seeding strategy in a supercritical fluid reactor. Rational control over the branching morphology, including the branch density, wire length, and wire diameter, can be achieved by optimizing the reaction conditions. A colloidal dispersion of gold nanocrystals was used to grow the silicon nanowire backbones, while copper nanocrystals were used to achieve epitaxial growth of silicon branches due to the facile alloying of copper with crystalline silicon. Because the two reactions, one involving gold seeds and one involving copper seeds, are orthogonal, the growth process can be interrogated more easily. By using gold as the initial seed, we can take samples from each growth step and better understand the growth mechanism with a clear distinction between the reactions involving the two different seeds. Crystallinity and registry of the backbone and branches were confirmed by high-resolution transmission electron microscopy (HRTEM) and fast Fourier transforms (FFTs) of the resulting images.

Semiconductor nanowires are an extremely important class of nanomaterials, and have huge potential to serve as building blocks for bottom-up construction of nanoscale electronic and optoelectronic devices[69], [104], [105]. Over the past two decades, various synthesis techniques have been developed and improved upon for the growth of semiconductor nanowires.[105]–[108] These techniques offer the flexibility to vary composition and morphology, thereby opening up many opportunities for fundamental research studies on silicon nanowires and applications in transistors[1]–[8], biological sensors[9], [10] and photovoltaic devices[13]–[17].

Branched nanowires offer an additional platform for increasing structural complexity and enabling greater functionality. Three-dimensional nanowire architectures can be achieved by branch growth or nanowire kinking during growth. Branched nanowire structures, sometimes referred to as nanotrees, can be constructed by growing branches epitaxially on the sidewalls of nanowire trunks. In recent years, several advanced morphologies have been achieved, with helical nanotree growth[42], [64], hyper-branch growth[18], [19], [41], [65], [66], oscillation of the branch diameter[67], [68] and controlled branch placement[55]–[57] being reported. With the clear advancement in control of branched nanowire morphologies on a lab scale, one clear next step is to enable the large-scale production of branched nanowires. As discussed previously, supercritical-fluid based growth techniques have clear advantages in large-scale nanowire production.

The sequential deposition of a suitable metal catalyst followed by vapor–liquid–solid (VLS), solution–liquid–solid (SLS), or other catalyst-driven nanowire growth might be the simplest method of nanowire branching. Copper is well known to be one of the fastest diffusing elements in silicon, enabling the facile alloying of copper structures with silicon. The diffusion of copper in silicon obeys the Arrhenius law, with $D(Cu) = 4.7 \times 10^{-3} \exp(-0.43 \text{ eV}/kT) \text{ cm}^2\text{s}^{-1}$ [109]. In super-critical-fluid based growth of silicon nanowires, once the backbone is established via gold-seeded growth, copper nanocrystals are introduced as branch seeds. In this reaction, copper will alloy with the silicon nanowire backbone to form copper silicide particles and seed the formation of epitaxial silicon nanowire branches grown from the connection. By separating the synthesis into the initial reaction involving gold seeds and the branch growth reaction involving copper, the growth mechanism of the copper seeded branches becomes more clear.

3.2 EXPERIMENTAL METHODS

A nitrogen-filled glove box (H_2O < 0.5 ppm, O_2 < 0.5 ppm) was used to store and handle all air- and moisture-sensitive chemicals. All copper nanocrystal syntheses were carried out under nitrogen atmosphere using standard Schlenk line techniques.

3.2.1 *Materials and Reagents*

Monophenylsilane (>95%) was purchased from Gelest. Toluene (anhydrous, 99.8%) was purchased from Sigma-Aldrich. Chloroform (HPLC grade, 99.9%) and toluene (Certified ACS, 99.8%) were purchased from Fisher Chemistry. Ethanol (200 proof) was purchased from Decon Laboratories.

3.2.2 *Two-Step Synthesis of Branched Silicon Nanowires*

1-Dodecanethiol (DDT)-passivated gold (Au) nanocrystals were prepared in deionized water and toluene via the method of Brust *et al.* [110]. 1-Dodecylamine (DDA)-capped copper nanocrystals were prepared by the method of Ben Aissa *et al*.[96]. Au-seeded Si nanowires were prepared by the supercritical fluid-liquid-solid (SFLS) growth process, as described in Chapter 2.[111] A 12-mL solution of anhydrous toluene containing 40 mg/L Au nanocrystals and 54 mM monophenylsilane was prepared in a nitrogen-filled glovebox. A 10-mL nitrogen-filled titanium flow-through reactor was heated to 490°C, filled with anhydrous toluene, and pressurized to 1500 psig using a high-performance liquid chromatography (HPLC) pump. After the reactor had equilibrated at the desired temperature and pressure, the nanocrystal/precursor solution was loaded into a 10-ml injection loop connected to the six-way injection valve. Nanowire growth was carried out by using the HPLC pump to inject the Au nanocrystal and monophenylsilane precursor solution into the reactor at a rate of 0.5 mL/min for 20 min. After the growth of Au-seeded Si nanowires,

the HPLC pump continued to inject anhydrous toluene into the reactor to flush away non-reactive residue for 10 minutes. The reactor was then heated to 550°C, and Cu nanocrystals were loaded into the injection loop, and gradually introduced to the reactor. After this step, silicon precursor was introduced into the reactor once again in order to promote the continuous growth of epitaxial silicon branches.

3.2.3 *Characterization Methods*

Transmission Electron Microscopy (TEM)

Transmission electron microscope (TEM) images were acquired with a FEI Technai G2 F20 Super Twin TEM, operating at 200 kV. Digital Micrograph software was used to analyze Fast Fourier Transforms (FFTs) of high-resolution TEM images. TEM samples were prepared by dropcasting 8 μL of nanocrystal/nanowire dispersion in organic solvents onto either carbon-coated copper TEM grids or carbon-coated 200 mesh nickel TEM grids inside of the glovebox.

Energy Dispersive X-ray Spectroscopy (EDS)

Energy-dispersive X-ray spectroscopy (EDS) was carried out using a transmission electron microscope (FEI Technai G2 F20) equipped with an X-ray energy-dispersive spectroscopy detector (EDAX Element Silicon Drift Detector) in order to analyze the seed and nanowire compositions.

Scanning Electron Microscopy (SEM)

To characterize the morphology of the nanowires, scanning electron microscopy (SEM) images were acquired with a FEI XL830 Dual Beam FIB/SEM. Samples were prepared by drop-casting nanowires onto pre-cleaned silicon wafer substrates.

Inductively Coupled Plasma Atomic Emission Spectroscopy (ICP-AES)

To determine the concentration of copper nanocrystals, inductively coupled plasma atomic emission spectroscopy (ICP-AES) analysis was performed using a Perkin Elmer Optima 8300. Nanocrystals were digested in *aqua regia* prepared from ultrapure nitric acid and hydrochloric acid in a 1:3 volume ratio. Once digestion was complete, samples were diluted using (18.2 MΩ) deionized water. Calibrations were performed using multi-element VII ICP-AES standards obtained from EMD Millipore.

3.3 Results and Discussion

We sought to elucidate the growth mechanism of copper seeded branched silicon nanowires with chemical intuition. In order to be able to separate the branch growth from the silicon nanowire backbone growth, we chose the widely established gold catalyst system as the seed for the silicon nanowire backbone. Then copper was used as the second catalyst to facilitate alloying with the SiNW backbone to then form copper silicide nucleation sites. With a continuous introduction of silicon precursor, the alloyed copper silicide particles then facilitated growth of epitaxial SiNW branches with crystallographic registry. With different catalysts for backbone and branches, we were able to separate each growth step and track the growth process.

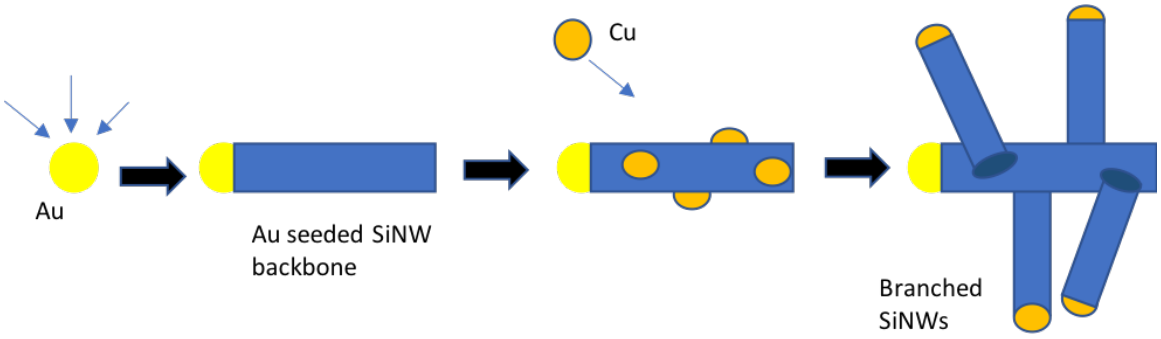

The growth mechanism for Au and Cu co-seeded branched SiNWs can be illustrated as shown in Figure 3.1. First, the Au seeded SiNW backbones were synthesized at 363°C via SFLS growth. After the backbone growth process was complete, the reactor was flushed with supercritical toluene for 10 minutes to remove any unreacted residues and clean the wires. Then, a Cu NCs dispersion was injected into the reactor to alloy with the SiNW backbones and form copper silicide nucleation sites. Silicon nanowire branches are then grown from these copper silicide sites via the continuous injection of additional silicon precursor.

Figure 3.2 shows SEM images of as-synthesized SFLS-grown Au-seeded SiNWs. It is important to note that we do not observed any branched structures resulting from the SFLS-based Au-seeded SiNW growth step prior to the introduction of copper seeds.

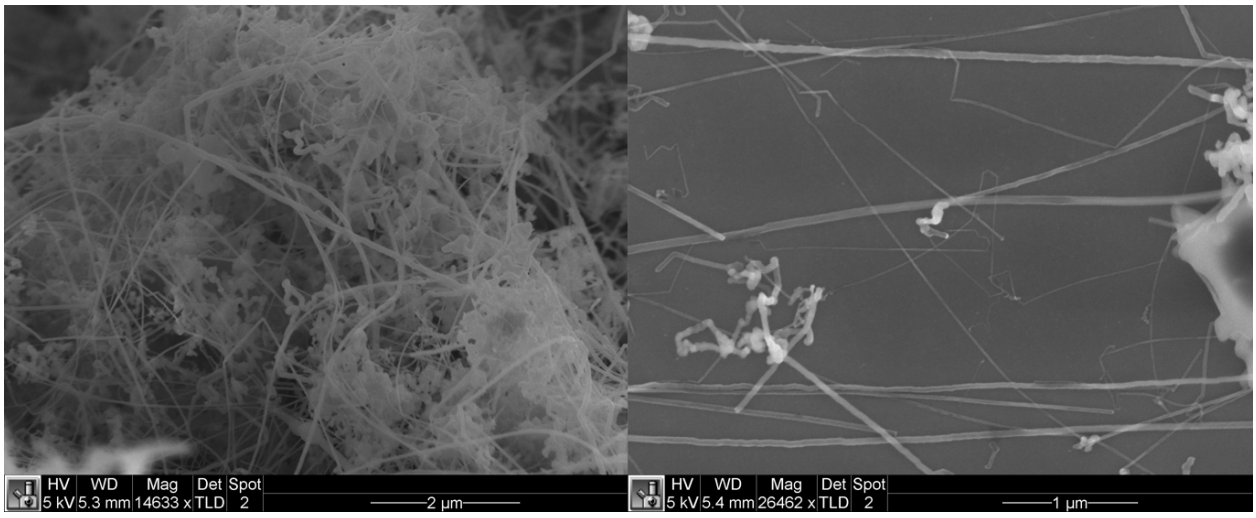

Figure 3.3 depicts TEM images of SFLS-grown Au-seeded SiNWs after the injection of Cu NCs. From these images, we can claim that after injection, the copper nanocrystals have clearly alloyed with the silicon nanowire backbones and formed copper silicide nucleation sites. An organic surface layer can also be clearly seen around both the wire and the copper silicide particle

in the high resolution TEM image in Figure 3.3.c and Figure 3.3.d, which also provides strong evidence to support alloying and our proposed epitaxial growth mechanism.

With the confirmation of Cu_3Si nucleation sites formed on the SiNW backbones, we continued the growth process by introducing additional silicon precursor into the system to encourage the growth of epitaxial SiNW branches from the copper silicide junction points. Due to the tangled nature and high density of the branched nanowire product, it was difficult to clearly identify branch points via SEM. However, after significant sonication of the product, it was possible to separate and image individual wire fragments that clearly demonstrate branching, as shown in Figure 3.4.

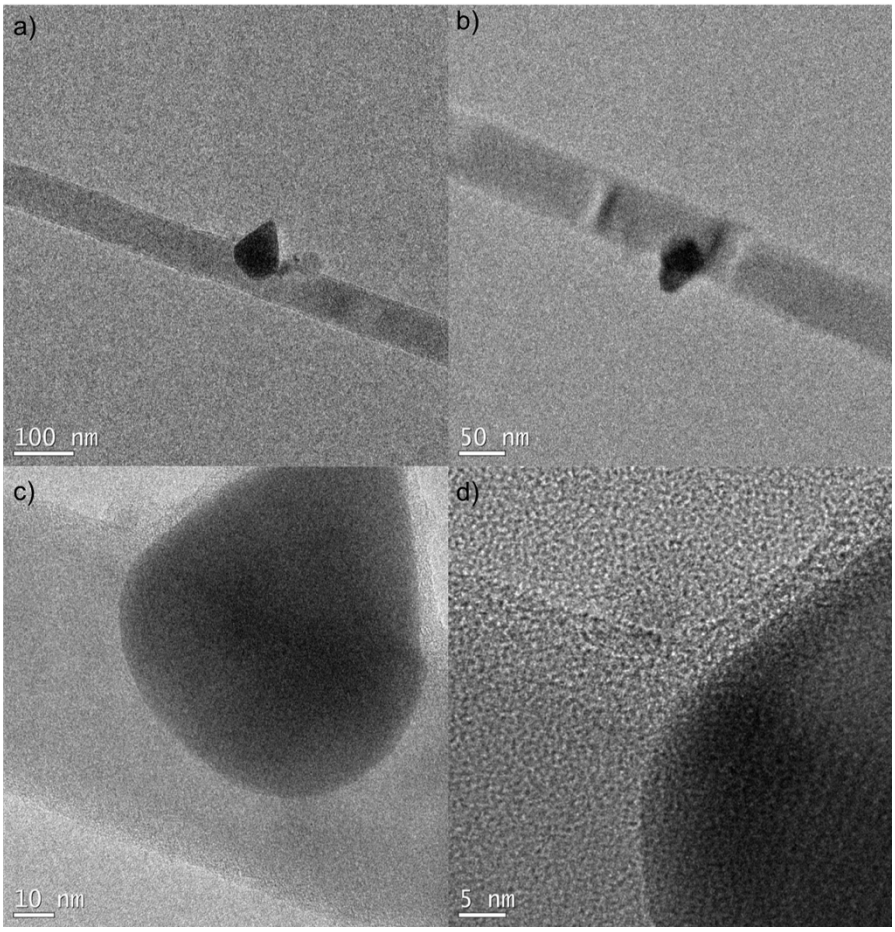

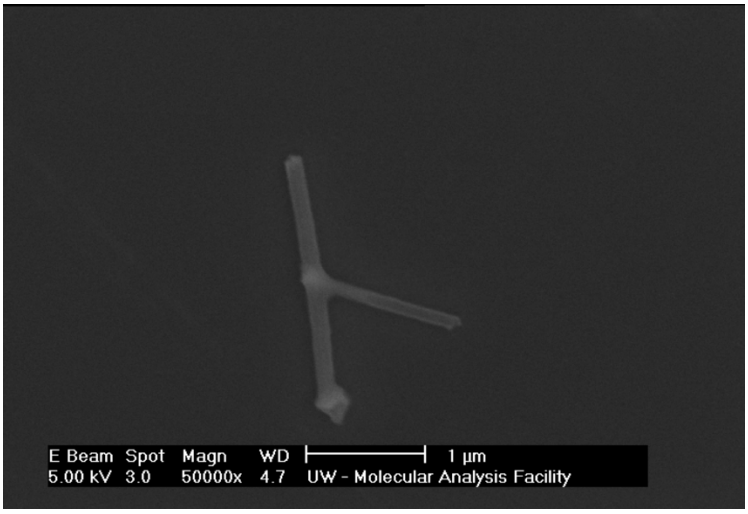

Figure 3.4 SEM images of single branched SiNW

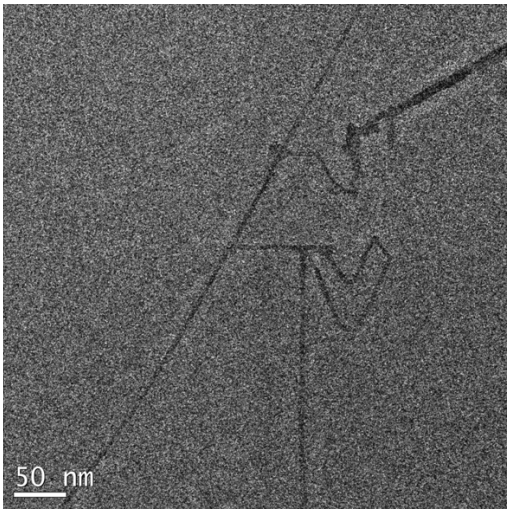

Figure 3.5 TEM images of branched SiNWs

Since a single SEM image is not convincing enough to prove that branched SiNWs were grown, extensive TEM and HRTEM analysis was used to study the branched NWs in depth and interrogate their crystal structures. Figure 3.5 presents a characteristic TEM image of Au-seeded SiNW backbones and Cu-seeded SiNW branches. These branched structures are clearly distinct from wires that are simply overlaid on top of each other (Appendix B in Figure B.1). Also, the

branches exhibit clear epitaxial relationships and crystallographic registry, as discussed in detail below. The data that follows indicates that epitaxial single-crystalline SFSS-grown Cu-seeded SiNW branches grow directly from the SFLS grown Au-seeded SiNW backbone. Branches are seeded epitaxially via the Cu_3Si nucleation sites formed by Cu NCs alloying with SiNWs at high temperature. Although precise control over the position of secondary Cu catalysts on the backbone has not yet been achieved in a supercritical fluid reactor, the density of branches on the nanowires could likely be controlled by varying the concentration of Cu colloids used to seed the branch growth.

The facile alloying of copper with crystalline silicon is the key for the epitaxial growth of branches. With the knowledge gathered from the above study, we can now propose a one-step synthesis of branched single crystalline Cu-seeded SiNWs. The growth procedure is similar to the procedure used in Chapter 2 for Cu-seeded SiNW growth. We attempted growing branched silicon nanowires with a continuous feed of seed and precursor solution, but with a time gradient for the addition of Cu to the reactor. Using this method, branched SiNWs were expected to grow whenever a Cu NC came in contact with an already-grown SiNW.

Figure 3.6 shows the TEM and HRTEM images of branched silicon nanowires from the one-step synthesis using copper nanocrystals as seed materials. As shown in the figure, two branches with triangular seeds are clearly connected. HRTEM images were once again used to obtain information regarding the crystallinity of the branches and connection, clearly showing the single-crystalline epitaxial nature and crystallographic registry of both the backbone and the branches.

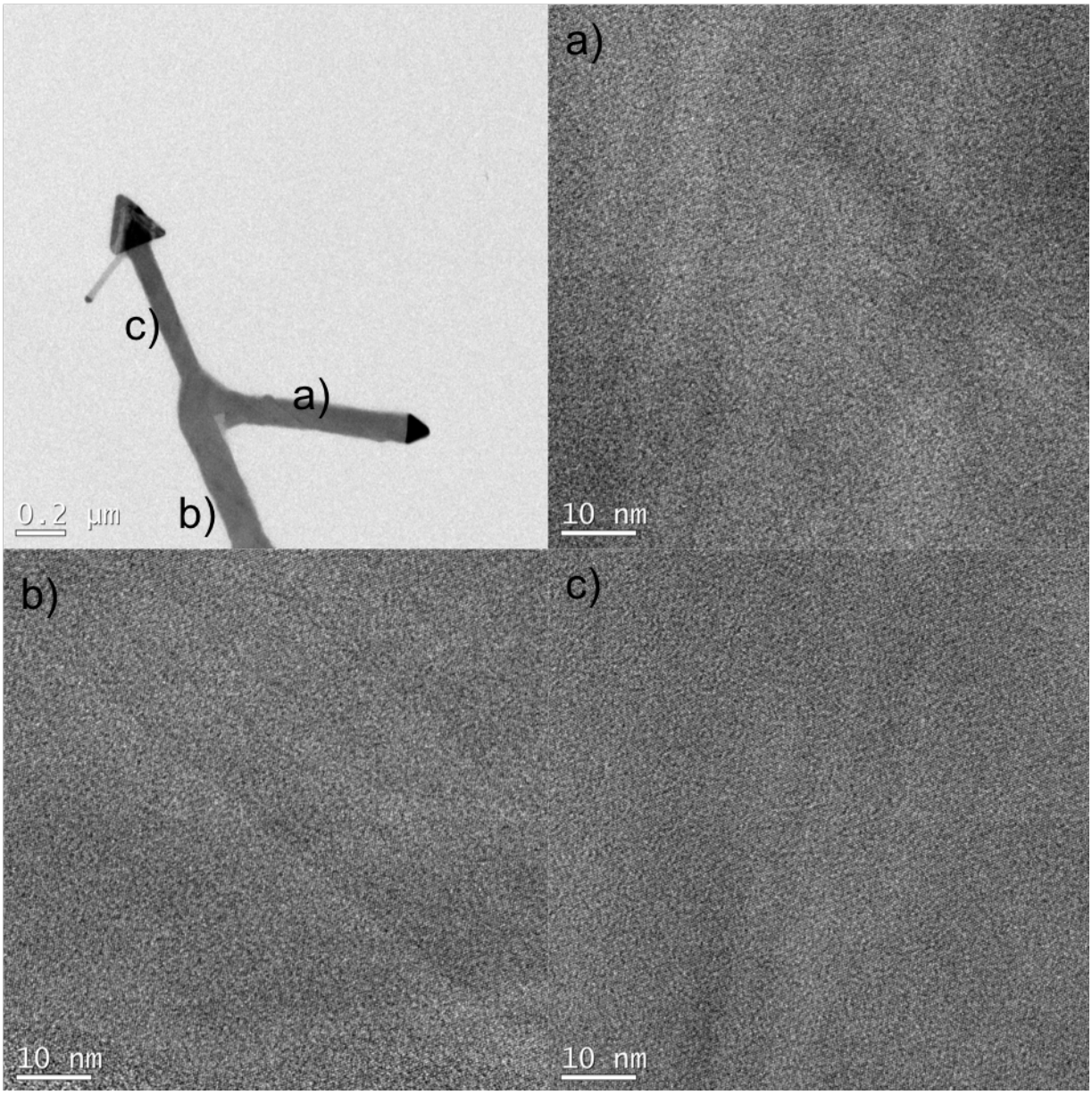

Figure 3.6 TEM and HRTEM of Cu-seeded SiNW branches

The Cu/Si binary phase diagram shows a eutectic temperature of 802°C, which is higher than the reaction temperature of 550°C, indicating that the obtained silicon nanowires grew from catalyst seeds in the solid state. With the catalyst particles being larger than 10 nm, a significantly reduced melting temperature is not expected[103]. This is another indication that in this case, the nanowire growth occurred in the SFSS regime. The large, triangular-shaped tip can therefore likely

be ascribed to the aggregation of copper seeds, followed by subsequent alloying. Branched wire growth can be explained by the facile alloying of copper with crystalline silicon combined with the continuous introduction of copper seeds throughout the duration of the growth process. Because copper was introduced into the reactor gradually, during the later stages of growth, there will already be silicon nanowires that were grown during an earlier stage. When a copper nanocrystal comes into contact with one of these previously grown silicon nanowires, it will quickly alloy and form a copper silicide nucleation site. With a continuous supply of silicon precursor to the reactor, more silicon is then incorporated into copper silicide and eventually a new epitaxial silicon branch grows from the connection.

3.4 CONCLUSIONS

In this chapter, we discussed the effects of copper alloying on branched nanowire formation by tracing the changes in each growth step by using distinguishable metal seeds. We presented a one-step method to grow single-crystalline branched silicon nanowires by taking advantage of the facile alloying of copper with crystalline silicon. This study shows that the growth direction and composition of branched silicon nanowires can be tailored by the choice of catalyst and precursor. This approach can potentially be adapted to integrate different materials into the backbone/branch heterostructures. This provides further control over nanowire morphology, giving an additional handle to explore and design nanowires for various applications.

REFERENCES

[1] A. Heinzig, S. Slesazeck, F. Kreupl, T. Mikolajick, and W. M. Weber, "Reconfigurable Silicon Nanowire Transistors," *Nano Lett.*, vol. 12, no. 1, pp. 119–124, Jan. 2012.

[2] N. Clément and G. Larrieu, "Electronic transport mechanisms in scaled gate-all-around silicon nanowire transistor arrays," *Appl. Phys. Lett.*, vol. 103, no. 26, p. 263504, Dec. 2013.

[3] J. Wallentin, M. Ek, L. R. Wallenberg, L. Samuelson, and M. T. Borgström, "Electron Trapping in InP Nanowire FETs with Stacking Faults," *Nano Lett.*, vol. 12, no. 1, pp. 151–155, Jan. 2012.

[4] K. Tomioka, M. Yoshimura, and T. Fukui, "A III–V nanowire channel on silicon for high-performance vertical transistors," *Nature*, vol. 488, no. 7410, pp. 189–192, Aug. 2012.

[5] J. Xiang, W. Lu, Y. Hu, Y. Wu, H. Yan, and C. M. Lieber, "Ge/Si nanowire heterostructures as high-performance field-effect transistors," *Nature*, vol. 441, no. 7092, pp. 489–493, May 2006.

[6] M. Singh Parihar, D. Ghosh, and A. Kranti, "Single transistor latch phenomenon in junctionless transistors," *J. Appl. Phys.*, vol. 113, no. 18, p. 184503, May 2013.

[7] W. Lu, P. Xie, and C. M. Lieber, "Nanowire Transistor Performance Limits and Applications," *IEEE Trans. Electron Devices*, vol. 55, no. 11, pp. 2859–2876, Nov. 2008.

[8] K. A. Dick *et al.*, "Directed growth of branched nanowire structures," *MRS Bull.*, vol. 32, no. 2, pp. 127–133, 2007.

[9] Y. Cui, "Species Selective Detection of Biological and Chemical Nanowire Nanosensors for Highly Sensitive and," 2006.

[10] J. H. and and C. M. Lieber*, "Direct Ultrasensitive Electrical Detection of DNA and DNA Sequence Variations Using Nanowire Nanosensors," 2003.

[11] F. Patolsky and C. M. Lieber, "Nanowire nanosensors," *Mater. Today*, vol. 8, no. 4, pp. 20–28, Apr. 2005.

[12] Q. Wan and T. H. Wang, "Single-crystalline Sb-doped SnO2 nanowires: synthesis and gas sensor application," *Chem. Commun.*, vol. 0, no. 30, p. 3841, Jul. 2005.

[13] N. Anttu *et al.*, "Third generation photovoltaics: Ultra-high conversion efficiency at low cost," *IEEE J. Sel. Top. Quantum Electron*, vol. 5, no. 3, pp. 1050–1061, 2006.

[14] J. Wallentin *et al.*, "InP Nanowire Array Solar Cells Achieving 13.8% Efficiency by Exceeding the Ray Optics Limit," *Science (80-.).*, vol. 339, no. 6123, pp. 1057–1060, Mar. 2013.

[15] T. J. Kempa, R. W. Day, S.-K. Kim, H.-G. Park, and C. M. Lieber, "Semiconductor nanowires: a platform for exploring limits and concepts for nano-enabled solar cells," *Energy Environ. Sci.*, vol. 6, no. 3, p. 719, Feb. 2013.

[16] E. C. Garnett, M. L. Brongersma, Y. Cui, and M. D. McGehee, "Nanowire Solar Cells," *Annu. Rev. Mater. Res.*, vol. 41, no. 1, pp. 269–295, Aug. 2011.

[17] A. I. Hochbaum and P. Yang, "Semiconductor Nanowires for Energy Conversion," *Chem. Rev.*, vol. 110, no. 1, pp. 527–546, Jan. 2010.

[18] A. R. Bielinski *et al.*, "Rational Design of Hyperbranched Nanowire Systems for Tunable Superomniphobic Surfaces Enabled by Atomic Layer Deposition," *ACS Nano*, vol. 11, no. 1, pp. 478–489, Jan. 2017.

[19] J. Zhu, H. Peng, C. K. Chan, K. Jarausch, X. F. Zhang, and Y. Cui, "Hyperbranched Lead Selenide Nanowire Networks," *Nano Lett.*, vol. 7, no. 4, pp. 1095–1099, Apr. 2007.

[20] H. Kim and J. Cho, “Superior Lithium Electroactive Mesoporous Si@Carbon Core−Shell Nanowires for Lithium Battery Anode Material,” *Nano Lett.*, vol. 8, no. 11, pp. 3688–3691, Nov. 2008.
[21] J. Chen, L. Yang, S. Rousidan, S. Fang, Z. Zhang, and S. Hirano, “Facile fabrication of Si mesoporous nanowires for high-capacity and long-life lithium storage,” *Nanoscale*, vol. 5, no. 21, p. 10623, Oct. 2013.
[22] † Candace K. Chan, ‡ and Xiao Feng Zhang, and £ Yi Cui*, “High Capacity Li Ion Battery Anodes Using Ge Nanowires,” 2007.
[23] J. Y. Huang *et al.*, “In Situ Observation of the Electrochemical Lithiation of a Single SnO_2 Nanowire Electrode,” *Science (80-.).*, vol. 330, no. 6010, pp. 1515–1520, Dec. 2010.
[24] L.-F. Cui, R. Ruffo, C. K. Chan, H. Peng, and Y. Cui, “Crystalline-Amorphous Core−Shell Silicon Nanowires for High Capacity and High Current Battery Electrodes,” *Nano Lett.*, vol. 9, no. 1, pp. 491–495, Jan. 2009.
[25] M. Ben-Ishai and F. Patolsky, “A Route to High-Quality Crystalline Coaxial Core/Multishell Ge@Si(GeSi) *n* and Si@(GeSi) *n* Nanowire Heterostructures,” *Adv. Mater.*, vol. 22, no. 8, pp. 902–906, Feb. 2010.
[26] T. Ozel, B. Zhang, R. Gao, R. W. Day, C. M. Lieber, and D. G. Nocera, “Electrochemical Deposition of Conformal and Functional Layers on High Aspect Ratio Silicon Micro / Nanowires Electrochemical Deposition of Conformal and Functional Layers on High Aspect Ratio Silicon Micro / Nanowires,” *Nano Lett.*, pp. 1–26, 2017.
[27] Y. Liu, S. Vishniakou, J. Yoo, and S. A. Dayeh, “Engineering Heteromaterials to Control Lithium Ion Transport Pathways,” *Sci. Rep.*, vol. 5, no. 1, p. 18482, Nov. 2016.
[28] C. K. Kamaja, M. Rajaperumal, R. Boukherroub, and M. V. Shelke, “Silicon Nanostructures-Graphene Nanocomposites,” pp. 176–195.
[29] M. J. Bierman and S. Jin, “Potential applications of hierarchical branching nanowires in solar energy conversion,” *Energy Environ. Sci.*, vol. 2, no. 10, pp. 1050–1059, 2009.
[30] R. Ghosh and P. K. Giri, “Silicon nanowire heterostructures for advanced energy and environmental applications: a review,” *Nanotechnology*, vol. 28, no. 1, p. 012001, Jan. 2017.
[31] S. Noor Mohammad, “Why self-catalyzed nanowires are most suitable for large-scale hierarchical integrated designs of nanowire nanoelectronics,” *J. Appl. Phys.*, vol. 110, no. 8, p. 084310, Oct. 2011.
[32] J. L. Pura, P. Periwal, T. Baron, and J. Jiménez, “Growth dynamics of SiGe nanowires by the vapour-liquid-solid method and its impact on SiGe/Si axial heterojunction abruptness,” *Nanotechnology*, vol. 29, no. 35, p. 355602, 2018.
[33] B. Eisenhawer, V. Sivakov, A. Berger, and S. Christiansen, “Growth of axial SiGe heterostructures in nanowires using pulsed laser deposition,” *Nanotechnology*, vol. 22, no. 30, 2011.
[34] F. Wen and E. Tutuc, “Enhanced Electron Mobility in Nonplanar Tensile Strained Si Epitaxially Grown on $Si_x Ge_{1-x}$ Nanowires,” *Nano Lett.*, p. acs.nanolett.7b03450, 2017.
[35] E. Mullane, H. Geaney, and K. M. Ryan, “Synthesis of silicon–germanium axial nanowire heterostructures in a solvent vapor growth system using indium and tin catalysts,” *Phys. Chem. Chem. Phys.*, vol. 17, no. 10, pp. 6919–6924, Feb. 2015.
[36] Y.-T. Wu *et al.*, “Nickel/Platinum Dual Silicide Axial Nanowire Heterostructures with Excellent Photosensor Applications,” *Nano Lett.*, vol. 16, no. 2, pp. 1086–1091, Feb. 2016.

[37] H. Geaney, E. Mullane, Q. M. Ramasse, and K. M. Ryan, “Atomically Abrupt Silicon–Germanium Axial Heterostructure Nanowires Synthesized in a Solvent Vapor Growth System,” *Nano Lett.*, vol. 13, no. 4, pp. 1675–1680, Apr. 2013.
[38] H. Yuan *et al.*, “Axial heterostructure of Au-catalyzed InGaAs/GaAs nanowires grown by metal-organic chemical vapor deposition,” *Chem. Phys. Lett.*, vol. 692, pp. 28–32, Jan. 2018.
[39] V. G. Dubrovskii, “A model of axial heterostructure formation in III–V semiconductor nanowires,” *Tech. Phys. Lett.*, vol. 42, no. 3, pp. 332–335, Mar. 2016.
[40] A. Koryakin, N. Sibirev, H. Huang, X. Ren, and V. Dubrovskii, “As flux controlled formation of (Al,Ga)As axial nanowire heterostructures,” in *AIP Conference Proceedings*, 2016, vol. 1748, no. 1, p. 040002.
[41] W.-Q. Wu, H.-S. Rao, H.-L. Feng, H.-Y. Chen, D.-B. Kuang, and C.-Y. Su, “A family of vertically aligned nanowires with smooth, hierarchical and hyperbranched architectures for efficient energy conversion,” *Nano Energy*, vol. 9, pp. 15–24, Oct. 2014.
[42] M. J. Bierman, Y. K. A. Lau, A. V. Kvit, A. L. Schmitt, and S. Jin, “Dislocation-Driven Nanowire Growth and Eshelby Twist,” *Science (80-.).*, vol. 320, no. 5879, pp. 1060–1063, May 2008.
[43] K. A. Dick *et al.*, “Synthesis of branched ‘nanotrees’ by controlled seeding of multiple branching events,” *Nat. Mater.*, vol. 3, no. 6, pp. 380–384, 2004.
[44] Y. Jung, D. K. Ko, and R. Agarwal, “Synthesis and structural characterization of single-crystalline branched nanowire heterostructures,” *Nano Lett.*, vol. 7, no. 2, pp. 264–268, 2007.
[45] R. Yang, Y. L. Chueh, J. R. Morber, R. Snyder, L. J. Chou, and Z. L. Wang, “Single-crystalline branched zinc phosphide nanostructures: Synthesis, properties, and optoelectronic devices,” *Nano Lett.*, vol. 7, no. 2, pp. 269–275, 2007.
[46] J. X. Wang *et al.*, “Growth of SnO2nanowires with uniform branched structures,” *Solid State Commun.*, vol. 130, no. 1–2, pp. 89–94, 2004.
[47] A. L. Beaudry *et al.*, “Directed branch growth in aligned nanowire arrays,” *Nano Lett.*, vol. 14, no. 4, pp. 1797–1803, 2014.
[48] G. S. Doerk, N. Ferralis, C. Carraro, and R. Maboudian, “Growth of branching Si nanowires seeded by Au-Si surface migration,” *J. Mater. Chem.*, vol. 18, no. 44, pp. 5376–5381, 2008.
[49] A. Dong, R. Tang, and W. E. Buhro, “Solution-based growth and structural characterization of homo- and heterobranched semiconductor nanowires,” *J. Am. Chem. Soc.*, vol. 129, no. 40, pp. 12254–12262, 2007.
[50] D. Wang, F. Qian, C. Yang, Z. Zhong, and C. M. Lieber, “Rational growth of branched and hyperbranched nanowire structures,” *Nano Lett.*, vol. 4, no. 5, pp. 871–874, 2004.
[51] M. S. Song, S. Bin Choi, and Y. Kim, “Wurtzite ZnTe Nanotrees and Nanowires on Fluorine-Doped Tin Oxide Glass Substrates,” *Nano Lett.*, vol. 17, no. 7, pp. 4365–4372, 2017.
[52] S. Lv *et al.*, “Enhanced Field Emission Performance of Hierarchical ZnO/Si Nanotrees with Spatially Branched Heteroassemblies,” *ACS Appl. Mater. Interfaces*, vol. 7, no. 24, pp. 13564–13568, Jun. 2015.
[53] X. Jiang *et al.*, “Rational growth of branched nanowire heterostructures with synthetically encoded properties and function.,” *Proc. Natl. Acad. Sci. USA*, vol. 108, no. 30, pp. 12212–6, Jul. 2011.

[54] W. Lu and C. M. Lieber, "Semiconductor nanowires," *J. Phys. D. Appl. Phys.*, vol. 39, no. 21, pp. R387–R406, Nov. 2006.
[55] K. A. Dick, K. Deppert, L. S. Karlsson, W. Seifert, R. Wellenberg, and L. Samuelson, "Position-controlled interconnected InAs nanowire networks," *Nano Lett.*, vol. 6, no. 12, pp. 2842–2847, 2006.
[56] K. Jun and J. M. Jacobson, "Programmable Growth of Branched Silicon Nanowires Using a Focused Ion Beam," *Nano Lett.*, vol. 10, no. 8, pp. 2777–2782, Aug. 2010.
[57] K. A. Dick, K. Deppert, M. W. Larsson, W. Seifert, L. R. Wallenberg, and L. Samuelson, "Height-controlled nanowire branches on nanotrees using a polymer mask," *Nanotechnology*, vol. 18, no. 3, p. 035601, Jan. 2007.
[58] C. K. Chan *et al.*, "High-performance lithium battery anodes using silicon nanowires," *Nat. Nanotechnol.*, vol. 3, no. 1, pp. 31–35, Jan. 2008.
[59] Y. He, X. Yu, Y. Wang, H. Li, and X. Huang, "Alumina-Coated Patterned Amorphous Silicon as the Anode for a Lithium-Ion Battery with High Coulombic Efficiency," *Adv. Mater.*, vol. 23, no. 42, pp. 4938–4941, Nov. 2011.
[60] H. Li, X. Huang, L. Chen, Z. Wu, and Y. Liang, "A High Capacity Nano-Si Composite Anode Material for Lithium Rechargeable Batteries," 1999.
[61] U. Kasavajjula, C. Wang, and A. J. Appleby, "Nano- and bulk-silicon-based insertion anodes for lithium-ion secondary cells," *J. Power Sources*, vol. 163, no. 2, pp. 1003–1039, Jan. 2007.
[62] A. Franco Gonzalez, N.-H. Yang, and R.-S. Liu, "Silicon Anode Design for Lithium-Ion Batteries: Progress and Perspectives," *J. Phys. Chem. C*, vol. 121, no. 50, pp. 27775–27787, Dec. 2017.
[63] A. Casimir, H. Zhang, O. Ogoke, J. C. Amine, J. Lu, and G. Wu, "Silicon-based anodes for lithium-ion batteries: Effectiveness of materials synthesis and electrode preparation," *Nano Energy*, vol. 27, pp. 359–376, Sep. 2016.
[64] S. Jin, M. J. Bierman, and S. A. Morin, "A New Twist on Nanowire Formation: Screw-Dislocation-Driven Growth of Nanowires and Nanotubes," *J. Phys. Chem. Lett.*, vol. 1, no. 9, pp. 1472–1480, May 2010.
[65] Matthew J. Bierman, and Y. K. Albert Lau, and S. Jin*, "Hyperbranched PbS and PbSe Nanowires and the Effect of Hydrogen Gas on Their Synthesis," 2007.
[66] †,§ Deli Wang, †,§ Fang Qian, † Chen Yang, † and Zhaohui Zhong, and †,‡ Charles M. Lieber*, "Rational Growth of Branched and Hyperbranched Nanowire Structures," 2004.
[67] R. T. Tucker, A. L. Beaudry, J. M. LaForge, M. T. Taschuk, and M. J. Brett, "A little ribbing: Flux starvation engineering for rippled indium tin oxide nanotree branches," *Appl. Phys. Lett.*, vol. 101, no. 19, p. 193101, Nov. 2012.
[68] Y. Zhang, Y. Yan, and F. Zhu, "The Periodic Instability of Diameter of ZnO Nanowires via a Self-oscillatory Mechanism," *Nanoscale Res. Lett.*, vol. 2, no. 10, pp. 492–495, Sep. 2007.
[69] L. Samuelson, "Self-forming nanoscale devices," *Mater. Today*, vol. 6, no. 10, pp. 22–31, Oct. 2003.
[70] C. Thelander *et al.*, "Nanowire-based one-dimensional electronics," *Mater. Today*, vol. 9, no. 10, pp. 28–35, Oct. 2006.
[71] K.-J. Moon, T. Il Lee, W. Lee, and J.-M. Myoung, "White light emission from heterojunction diodes based on surface-oxidized porous Si nanowire arrays and amorphous In-Ga-Zn-O capping," *Nanoscale*, vol. 6, no. 7, p. 3611, Mar. 2014.

[72] D. A. Smith, V. C. Holmberg, and B. A. Korgel, “Flexible Germanium Nanowires: Ideal Strength, Room Temperature Plasticity, and Bendable Semiconductor Fabric,” *ACS Nano*, vol. 4, no. 4, pp. 2356–2362, Apr. 2010.
[73] Y. Zhu, F. Xu, Q. Qin, W. Y. Fung, and W. Lu, “Mechanical Properties of Vapor−Liquid−Solid Synthesized Silicon Nanowires,” *Nano Lett.*, vol. 9, no. 11, pp. 3934–3939, Nov. 2009.
[74] H.-P. Cheng, R. N. Barnett, and U. Landman, “Structure, collective hydrogen transfer, and formation of in clusters,” *J. Chem. Phys.*, vol. 116, p. 9191, 2002.
[75] X. . Zhou *et al.*, “Highly efficient and stable photoluminescence from silicon nanowires coated with SiC,” *Chem. Phys. Lett.*, vol. 332, no. 3–4, pp. 215–218, Dec. 2000.
[76] † Ling Pan, †,‡ Kok-Keong Lew, †,‡ and Joan M. Redwing, and †,‡ Elizabeth C. Dickey*, “Stranski−Krastanow Growth of Germanium on Silicon Nanowires,” 2005.
[77] Y.-C. Chou, C.-Y. Wen, M. C. Reuter, D. Su, E. A. Stach, and F. M. Ross, “Controlling the Growth of Si/Ge Nanowires and Heterojunctions Using Silver–Gold Alloy Catalysts,” *ACS Nano*, vol. 6, no. 7, pp. 6407–6415, Jul. 2012.
[78] M. Amato, M. Palummo, R. Rurali, and S. Ossicini, “Silicon–Germanium Nanowires: Chemistry and Physics in Play, from Basic Principles to Advanced Applications,” *Chem. Rev.*, vol. 114, no. 2, pp. 1371–1412, Jan. 2014.
[79] L. Chen, W. Y. Fung, and W. Lu, “Vertical Nanowire Heterojunction Devices Based on a Clean Si/Ge Interface,” *Nano Lett.*, vol. 13, no. 11, pp. 5521–5527, Nov. 2013.
[80] † Y. F. Zhang *et al.*, “Growth, Optical, and Electrical Properties of Single-Crystalline Si−CdSe Biaxial p−n Heterostructure Nanowires,” 2007.
[81] P. Sudhagar *et al.*, “High Open Circuit Voltage Quantum Dot Sensitized Solar Cells Manufactured with ZnO Nanowire Arrays and Si/ZnO Branched Hierarchical Structures,” *J. Phys. Chem. Lett.*, vol. 2, no. 16, pp. 1984–1990, Aug. 2011.
[82] C. Fang *et al.*, “Metallization of Silicon Nanowires and SERS Response from a Single Metallized Nanowire,” *Chem. Mater.*, vol. 21, no. 15, pp. 3542–3548, Aug. 2009.
[83] Y. Yu *et al.*, “ZIF-8 Cooperating in TiN/Ti/Si Nanorods as Efficient Anodes in Micro-Lithium-Ion-Batteries,” *ACS Appl. Mater. Interfaces*, vol. 8, no. 6, pp. 3992–3999, Feb. 2016.
[84] C. Duan, H. Wang, B. Zhang, F. Li, X. Ou, and X. Zhang, “Quantitative analysis of photons’ decaying pathways in Si nanowire arrays for highly efficient photoelectrochemical solar hydrogen generation,” *Chem. Commun.*, vol. 51, no. 16, pp. 3383–3386, Feb. 2015.
[85] J. M. Halpern, B. Wang, and H. Haick, “Controlling the Sensing Properties of Silicon Nanowires via the Bonds Nearest to the Silicon Nanowire Surface,” *ACS Appl. Mater. Interfaces*, vol. 7, no. 21, pp. 11315–11321, Jun. 2015.
[86] N. Liu, Y. Yao, J. J. Cha, M. T. McDowell, Y. Han, and Y. Cui, “Functionalization of silicon nanowire surfaces with metal-organic frameworks,” *Nano Res.*, vol. 5, no. 2, pp. 109–116, Feb. 2012.
[87] Y. Chen, X. Wang, S. Erramilli, P. Mohanty, and A. Kalinowski, “Silicon-based nanoelectronic field-effect pH sensor with local gate control,” *Appl. Phys. Lett.*, vol. 89, no. 22, p. 223512, Nov. 2006.
[88] G. D. Yuan *et al.*, “Tunable Electrical Properties of Silicon Nanowires *via* Surface-Ambient Chemistry,” *ACS Nano*, vol. 4, no. 6, pp. 3045–3052, Jun. 2010.
[89] V. Schmidt and B. Gutachter, “Silicon Nanowires : Synthesis , Fundamental Issues , and a

First Device," p. 141, 2006.
[90] B. M. Kayes, M. A. Filler, M. C. Putnam, M. D. Kelzenberg, N. S. Lewis, and H. A. Atwater, "Growth of vertically aligned Si wire arrays over large areas (>1 cm2) with Au and Cu catalysts," *Appl. Phys. Lett.*, vol. 91, no. 10, pp. 7–9, 2007.
[91] A. Richter, J. Benick, A. Fell, M. Hermle, and S. W. Glunz, "Impact of bulk impurity contamination on the performance of high-efficiency *n* -type silicon solar cells," *Prog. Photovoltaics Res. Appl.*, vol. 26, no. 5, pp. 342–350, May 2018.
[92] R. H. Hopkins and A. Rohatgi, "Impurity effects in silicon for high efficiency solar cells," *J. Cryst. Growth*, vol. 75, no. 1, pp. 67–79, May 1986.
[93] J. R. Davis *et al.*, "Impurities in silicon solar cells," *IEEE Trans. Electron Devices*, vol. 27, no. 4, pp. 677–687, Apr. 1980.
[94] D. C. Johnson, J. M. Mosby, S. C. Riha, and A. L. Prieto, "Synthesis of copper silicide nanocrystallites embedded in silicon nanowires for enhanced transport properties," *J. Mater. Chem.*, vol. 20, no. 10, pp. 1993–1998, 2010.
[95] M. Constantinou *et al.*, "Simultaneous Tunable Selection and Self-Assembly of Si Nanowires from Heterogeneous Feedstock," *ACS Nano*, vol. 10, no. 4, pp. 4384–4394, 2016.
[96] M. A. Ben Aissa, B. Tremblay, A. Andrieux-Ledier, E. Maisonhaute, N. Raouafi, and A. Courty, "Copper nanoparticles of well-controlled size and shape: A new advance in synthesis and self-organization," *Nanoscale*, 2015.
[97] L. L. Hung, C. K. Tsung, W. Huang, and P. Yang, "Room-temperature formation of hollow Cu2O nanoparticles," *Adv. Mater.*, vol. 22, no. 17, pp. 1910–1914, 2010.
[98] V. C. Holmberg and B. A. Korgel, "Corrosion resistance of thiol- and alkene-passivated germanium nanowires," *Chem. Mater.*, 2010.
[99] B. a Korgel, H. Y. Tuan, and A. Ghezelbash, "Silicon nanowires and silica nanotubes seeded by copper nanoparticles in an organic solvent," *Chem. Mater.*, vol. 20, no. 6, pp. 2306–2313, 2008.
[100] D. C. Lee, T. Hanrath, and B. A. Korgel, "The role of precursor-decomposition kinetics in silicon-nanowire synthesis in organic solvents," *Angew. Chemie - Int. Ed.*, vol. 44, no. 23, pp. 3573–3577, 2005.
[101] H.-Y. Tuan and B. A. Korgel, "Importance of Solvent-Mediated Phenylsilane Decompositon Kinetics for High-Yield Solution-Phase Silicon Nanowire Synthesis."
[102] V. T. Renard *et al.*, "Catalyst preparation for CMOS-compatible silicon nanowire synthesis," *Nat. Nanotechnol.*, vol. 4, no. 10, pp. 654–657, 2009.
[103] F. Delogu, "Structural and energetic properties of unsupported Cu nanoparticles from room temperature to the melting point: Molecular dynamics simulations," *Phys. Rev. B*, vol. 72, no. 20, p. 205418, Nov. 2005.
[104] C. M. Lieber, "Nanoscale Science and Technology: Building a Big Future from Small Things," *MRS Bull.*, vol. 28, no. 07, pp. 486–491, Jul. 2003.
[105] M. Law, J. Goldberger, and P. Yang, "SEMICONDUCTOR NANOWIRES AND NANOTUBES," *Annu. Rev. Mater. Res.*, vol. 34, no. 1, pp. 83–122, Aug. 2004.
[106] A. Li, J. Zou, and X. Han, "Growth of III-V semiconductor nanowires and their heterostructures," *Sci. China Mater.*, vol. 59, no. 1, pp. 51–91, 2016.
[107] M. M. Khayyat and B. Aïssa, "Si-NWs," pp. 108–130.
[108] F. Cansell and C. Aymonier, "Design of functional nanostructured materials using supercritical fluids," *J. Supercrit. Fluids*, vol. 47, no. 3, pp. 508–516, 2009.

[109] A. Mesli, T. Heiser, and E. Mulheim, “Copper diffusivity in silicon: A re-examination,” *Mater. Sci. Eng. B*, vol. 25, no. 2–3, pp. 141–146, Jul. 1994.
[110] M. Brust, M. Walker, D. Bethell, D. J. Schiffrin, and R. Whyman, “Synthesis of thiol-derivatised gold nanoparticles in a two-phase Liquid–Liquid system,” *J. Chem. Soc., Chem. Commun.*, no. 7, pp. 801–802, 1994.
[111] T. Hanrath and B. A. Korgel, “Supercritical fluid-liquid-solid (SFLS) synthesis of Si and Ge nanowires seeded by colloidal metal nanocrystals,” *Adv. Mater.*, 2003.

APPENDIX A

Gold Nanocrystal Synthesis:

2-nm diameter Au nanocrystals were prepared by the method of Brust *et al.*[110]. A 12.5-mL solution of 200 mM tetraoctylammonium bromide dissolved in toluene was combined with a 18-mL solution of 27 mM hydrogen tetrachloroaurate (III) trihydrate dissolved in deionized water and stirred vigorously for 30 minutes. The aqueous phase was then removed and discarded, and 0.5 mmol of 1-dodecanethiol was added to the solution, followed by a 15-mL solution of 0.4 M sodium borohydride in deionized water. The solution was allowed to stir for 2 hours and the organic phase was separated from the aqueous phase, which was discarded once again. The 2-nm diameter Au nanocrystals were precipitated via centrifugation using methanol as an antisolvent, dispersed in anhydrous toluene, and stored in a nitrogen-filled glove box.

Results from Preliminary Syntheses:

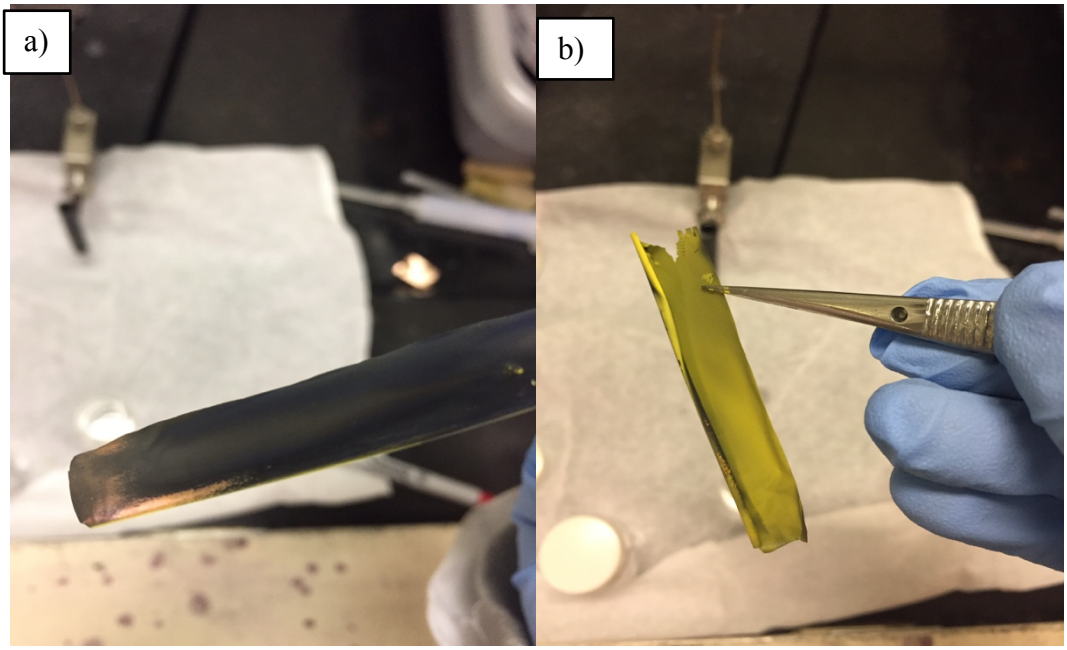

Figure A.1 front and back images of copper foil after SiNW synthesis. a) is the side faced downward toward the reactor wall, and b) is the side faced upward in the reactor

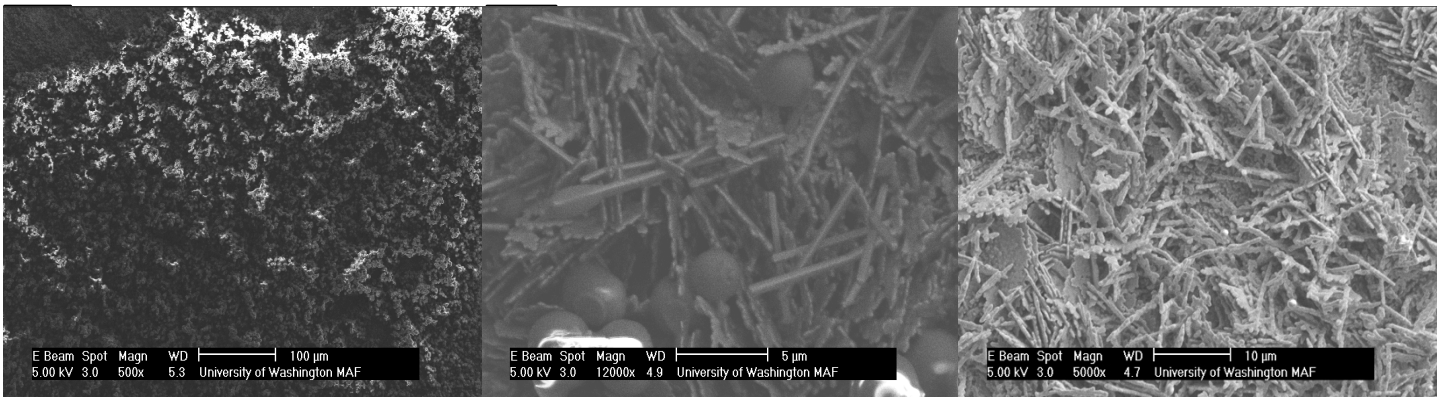

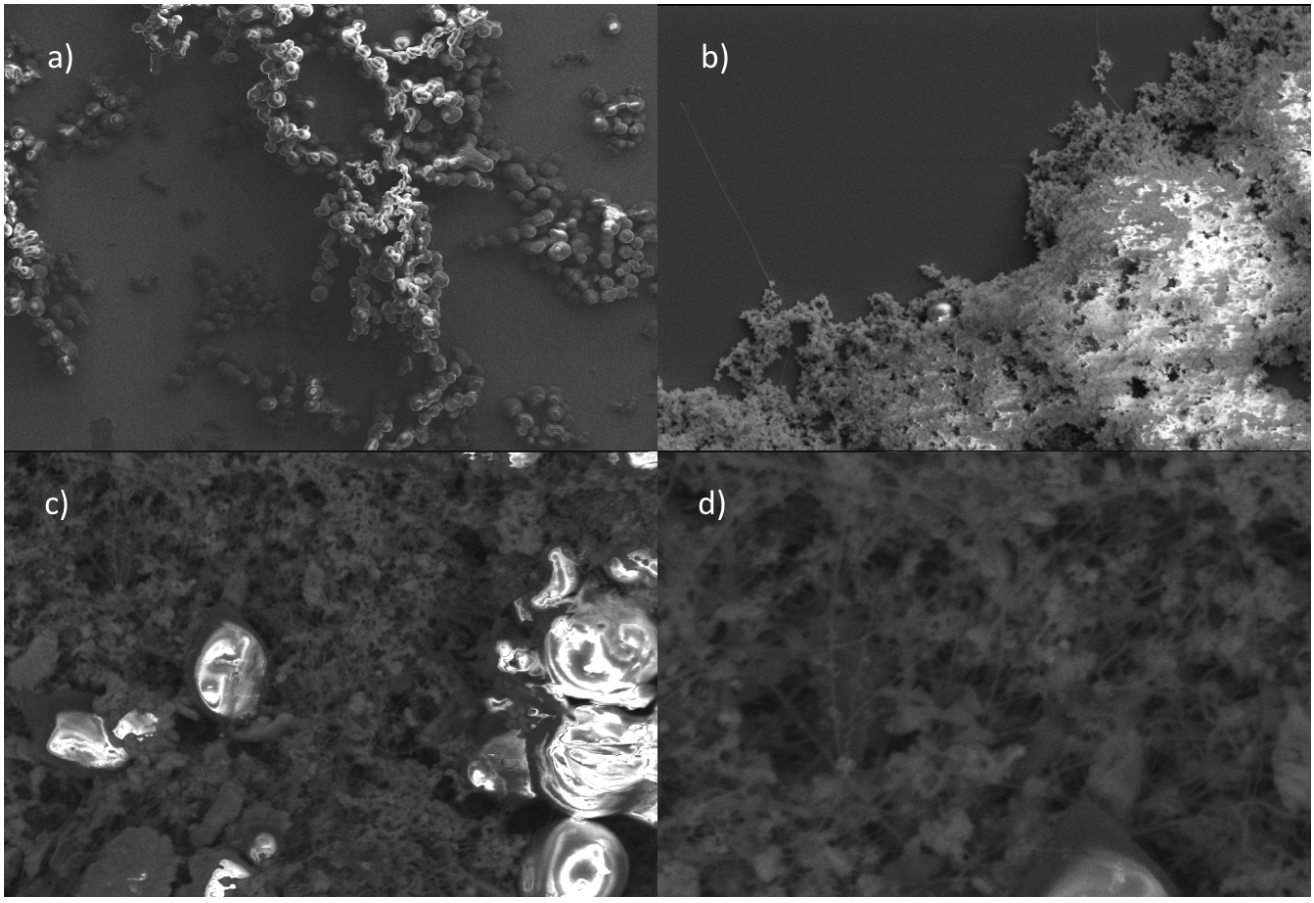

Figure A.2 SEM image

APPENDIX B

TEM images clearly show contrast differences as an indication that wires are crossed, not branched.

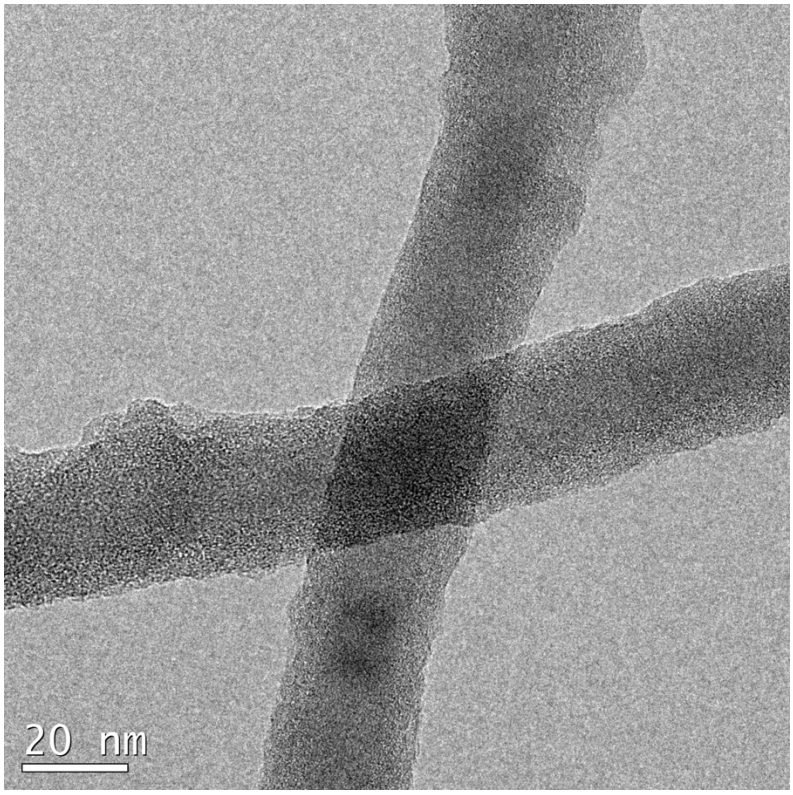

Figure B.1 TEM images of two separate crossed NWs overlaid on top of each other